TGF- Determines the Pro-migratory Potential of bFGF Signaling in Medulloblastoma

Santhana Kumar, Karthiga ; Neve, Anuja ; Guerreiro Stucklin, Ana S ; Kuzan-Fischer, Claudia M ; Rushing, Elisabeth J ; Taylor, Michael D ; Tripolitsioti, Dimitra ; Behrmann, Lena ; Kirschenbaum, Daniel ; Grotzer, Michael A ; Baumgartner, Martin

Abstract: The microenvironment shapes cell behavior and determines metastatic outcomes of tumors. We addressed how microenvironmental cues control tumor cell invasion in pediatric medulloblastoma (MB). We show that bFGF promotes MB tumor cell invasion through FGF receptor (FGFR) in vitro and that blockade of FGFR represses brain tissue infiltration in vivo. TGF- regulates pro-migratory bFGF function in a context-dependent manner. Under low bFGF, the non-canonical TGF- pathway causes ROCK activation and cortical translocation of ERK1/2, which antagonizes FGFR signaling by inactivating FGFR substrate 2 (FRS2), and promotes a contractile, non-motile phenotype. Under high bFGF, negative-feedback regulation of FRS2 by bFGF-induced ERK1/2 causes repression of the FGFR pathway. Under these conditions, TGF- counters inactivation of FRS2 and restores pro-migratory signaling. These findings pinpoint coincidence detection of bFGF and TGF- signaling by FRS2 as a mechanism that controls tumor cell invasion. Thus, targeting FRS2 represents an emerging strategy to abrogate aberrant FGFR signaling.

DOI: https://doi.org/10.1016/j.celrep.2018.05.083

Article

Cell Reports

TGF-β Determines the Pro-migratory Potential of bFGF Signaling in Medulloblastoma

Graphical Abstract

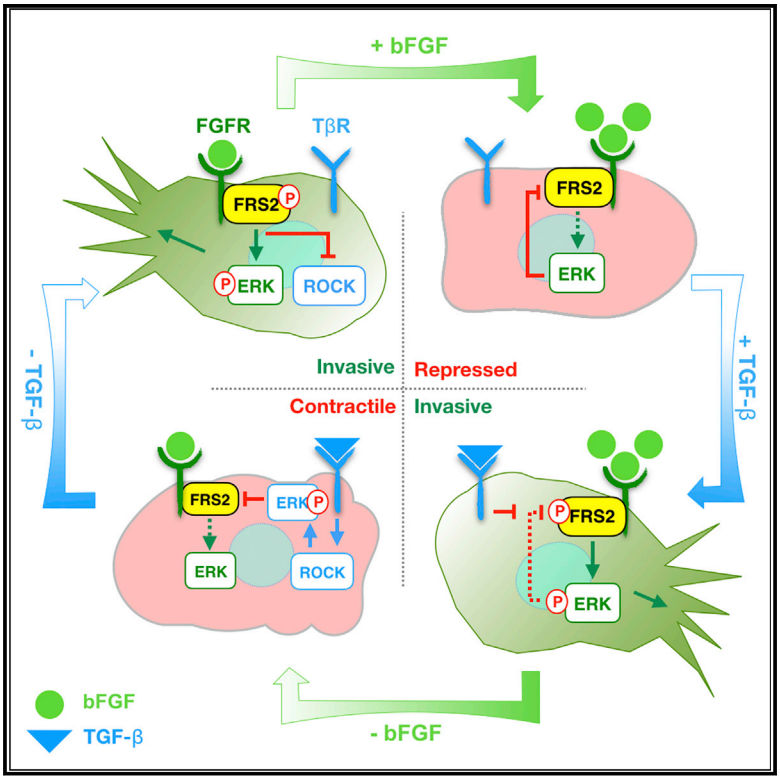

Authors

Karthiga Santhana Kumar, Anuja Neve, Ana S. Guerreiro Stucklin, ..., Daniel Kirschenbaum, Michael A. Grotzer, Martin Baumgartner

Correspondence

martin.baumgartner@kispi.uzh.ch

In Brief

Santhana Kumar et al. describe how growth factors in the microenvironment of medulloblastoma, the most common malignant brain tumor in children, are sensed by the tumor cells and how they respond to these factors. They identify the adaptor protein FRS2 as a key molecule controlling growth factor-induced tissue infiltration.

Highlights

- FGFR-FRS2 activation promotes brain tissue infiltration and tumor dissemination
- FRS2 integrates bFGF and TGF-β signaling to enable pro-invasive cell functions
- Non-canonical TGF-β signaling represses pro-invasive FGFR-FRS2 function
- TGF-β represses ERK-mediated negativefeedback regulation of FRS2

Santhana Kumar et al., 2018, Cell Reports *23*, 3798–3812
June 26, 2018
https://doi.org/10.1016/j.celrep.2018.05.083

CellPress

OPEN ACCESS
CellPress

Cell Reports
Article

TGF-β Determines the Pro-migratory Potential of bFGF Signaling in Medulloblastoma

Karthiga Santhana Kumar,[1] Anuja Neve,[1] Ana S. Guerreiro Stucklin,[2,3] Claudia M. Kuzan-Fischer,[2,5,7] Elisabeth J. Rushing,[4] Michael D. Taylor,[2,5,6,7] Dimitra Tripolitsioti,[1] Lena Behrmann,[8] Daniel Kirschenbaum,[4] Michael A. Grotzer,[1,9] and Martin Baumgartner[1,10,*]

[1]Paediatric Neuro-Oncology Research Group, Department of Oncology, Children's Research Center, University Children's Hospital Zürich, August-Forel Strasse 1, CH-8008 Zürich, Switzerland
[2]The Arthur and Sonia Labatt Brain Tumour Research Centre, The Hospital for Sick Children, Toronto, ON, Canada
[3]Division of Haematology/Oncology, The Hospital for Sick Children, Toronto, ON, Canada
[4]Institute of Neuropathology, University Hospital Zürich, Schmelzbergstrasse 12, CH-8091 Zürich, Switzerland
[5]Developmental and Stem Cell Biology Program, The Hospital for Sick Children, Toronto, ON, Canada
[6]Division of Neurosurgery, The Hospital for Sick Children, Toronto, ON, Canada
[7]Department of Surgery, Department of Laboratory Medicine and Pathobiology, and Department of Medical Biophysics, University of Toronto, Toronto, ON, Canada
[8]Paediatric Leukaemia Research Group, Department of Oncology, Children's Research Center, University Children's Hospital Zürich, August-Forel Strasse 1, CH-8008 Zürich, Switzerland
[9]Department of Oncology, University Children's Hospital Zürich, Steinwiesstrasse 75, CH-8032 Zürich, Switzerland
[10]Lead Contact
*Correspondence: martin.baumgartner@kispi.uzh.ch
https://doi.org/10.1016/j.celrep.2018.05.083

SUMMARY

The microenvironment shapes cell behavior and determines metastatic outcomes of tumors. We addressed how microenvironmental cues control tumor cell invasion in pediatric medulloblastoma (MB). We show that bFGF promotes MB tumor cell invasion through FGF receptor (FGFR) *in vitro* and that blockade of FGFR represses brain tissue infiltration *in vivo*. TGF-β regulates pro-migratory bFGF function in a context-dependent manner. Under low bFGF, the non-canonical TGF-β pathway causes ROCK activation and cortical translocation of ERK1/2, which antagonizes FGFR signaling by inactivating FGFR substrate 2 (FRS2), and promotes a contractile, non-motile phenotype. Under high bFGF, negative-feedback regulation of FRS2 by bFGF-induced ERK1/2 causes repression of the FGFR pathway. Under these conditions, TGF-β counters inactivation of FRS2 and restores pro-migratory signaling. These findings pinpoint coincidence detection of bFGF and TGF-β signaling by FRS2 as a mechanism that controls tumor cell invasion. Thus, targeting FRS2 represents an emerging strategy to abrogate aberrant FGFR signaling.

INTRODUCTION

Metastatic spread of tumor cells through tissue invasion is a hallmark of tumor progression. However, the contribution of microenvironment-derived growth factors to dissemination remains incompletely understood. We addressed this problem in medulloblastoma (MB), the most prevalent malignant pediatric brain tumor. MB tumor cells display an inherent propensity to infiltrate brain tissue and disseminate along the leptomeninges (Wu et al., 2012), which can lead to incurable disease and often causes disabling side effects of treatment in long-term survivors (Bouffet et al., 1992; Frühwald and Plass, 2002; Kiltie et al., 1997). Genome-wide DNA methylation and gene expression profiling has refined MB classification from four subgroups (Taylor et al., 2012) to a total of 12 subtypes (Cavalli et al., 2017; Schwalbe et al., 2017). Selected sonic hedgehog (SHH) subgroups have been found to align with high-risk, poor prognosis MB with the incidence of metastases varying greatly in all 12 subtypes. One cause for the aggressive behavior of MB tumors is local recurrence, which likely is the consequence of local brain infiltration. Nevertheless, the signaling pathways that promote tissue infiltration and metastasis remain poorly understood, thus limiting the discovery of rationally designed anti-metastatic targeting strategies in MB tumors.

Apart from intrinsic cellular factors, tumor progression and metastatic dissemination depend on the tumor microenvironment (Quail and Joyce, 2017). MB cause changes in extracellular matrix composition by increasing collagen IA deposition (Liang et al., 2008) and recruiting tumor-associated macrophages and leukocytes into the tumor microenvironment (Margol et al., 2015; Salsman et al., 2011). The impact of altered cellular composition and the manner by which growth factor and cytokine gradients control pro-invasive properties of the tumor cells are unknown. In other solid tumors, growth factors and concentration gradients within the tumor microenvironment define the extent of cancer cell dissemination (Bissell and Radisky, 2001; Wells et al., 2002). However, the mechanisms by which two or more growth factor signaling pathways regulate cancer cell dissemination remain poorly understood (Shirakihara et al., 2011; Snoussi et al., 2010).

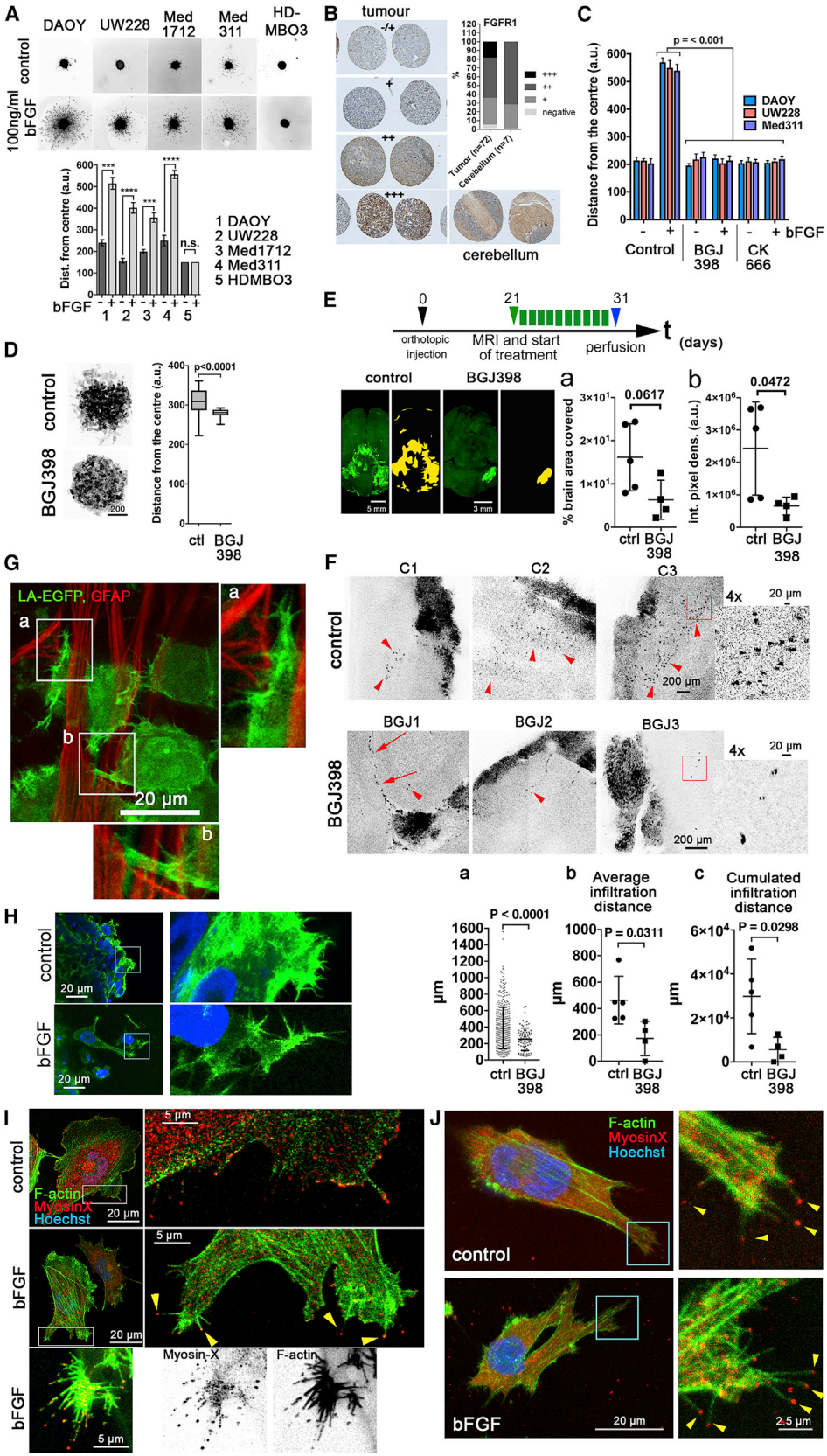

(legend on next page)

Using automated cell dissemination counter (aCDc), an unbiased platform for automated quantification of cell invasion, we identified basic fibroblast growth factor (bFGF, FGF2) as a strong promoter of MB cell migration and invasion (Kumar et al., 2015). bFGF was also found to inhibit SHH signaling and to block MB cell proliferation (Fogarty et al., 2007), and pre- or post-implantation exposure of orthotopically implanted MB tumor cells to high doses of bFGF impaired growth *in vivo* (Emmenegger et al., 2013). These potentially conflicting findings suggested that context-dependent bFGF signaling might determine MB progression to metastatic disease. We hypothesized that a reactive cellular environment with activated astrocytes, which secrete bFGF (Yang et al., 2014), could contribute to MB progression (Liu et al., 2017). Tumor-associated microglia could also generate a pro-migratory tumor microenvironment. Paradigmatic for such context-dependent signaling is transforming growth factor beta (TGF-β), which functions through SMAD-dependent and SMAD-independent non-canonical pathways (Ashcroft et al., 1999; Derynck and Zhang, 2003; Heldin et al., 2009; Massagué, 2012) and antagonizes SHH pathway functions in MB (Aref et al., 2013).

To determine the contribution of MB-associated growth factors and cytokines to tissue infiltration and tumor cell dissemination, this study investigated growth factor signaling and its effect on cancer cell invasion. Using patient-derived xenograft and genetically modified laboratory MB tumor lines, *ex vivo* organotypic cerebellum slice culture, and a human G3 MB xenograft model, we describe how cell invasion is regulated by variable levels of bFGF and how TGF-β signaling controls this process. The discovery of the rheostat regulation of fibroblast growth factor receptor (FGFR) signaling provides mechanistic understanding of context-dependent growth factor control of cell migration and invasion in health and disease.

RESULTS

Expression of FGFRs and bFGF in Human MB Tumor Tissue

We recently identified bFGF, the ligand of FGFRs, as a promoter of collagen I invasion in established SHH MB cell lines, in patient-derived xenografts (PDXs) of SHH and group 3 MB tumors, and in a PDX of a molecularly distinct, atypical MB (Kumar et al., 2015) Figure 1A). We observed no increase in invasion in response to bFGF in the group 3 MB cell line HD-MBO3 (Figure 1A). SHH and the PDX lines predominantly expressed FGFR1 at the mRNA level, except for HD-MBO3, which expressed FGFR4 (Figure S1A). Higher FGFR1 and FGFR4 mRNA levels were also observed in a small cohort of primary MB samples when compared to FGFR2 and FGFR3 (Figure S1B). To assess FGFR1 and FGFR4 protein abundance in human MB tissues, we analyzed a MB tissue microarray (TMA) by immunohistochemistry (IHC). We found that FGFR1 was expressed at low to moderate levels both in normal cerebellum (n = 7) adjacent to tumor and in the tumor (n = 72). 18% of the tumor tissues displayed high levels of FGFR1 expression (Figure 1B). Using the same approach, we were not able to detect FGFR4 in the same TMA (data not shown). We also detected FGFR1 by IHC in PDX models of group 3 and SHH MB, as well as in a primary tumor sample (Figure S1C). Interestingly, qRT-PCR detected only low mRNA expression levels of bFGF in MB cell lines and in PDX cells (Figure S1D). Consistently, only weak bFGF positivity was detected in tumor tissue (Figures S1E–S1H), suggesting that the available bFGF in the microenvironment is not derived from the tumor cells. However, we observed individual, strongly bFGF-positive cells within non-WNT/SHH MB tumor samples (Figure S1E), in the majority of MB TMA samples (Figure S1F), in a G3 MB PDX (Figure S1G), as well as in two additional MB validated clinical isolates (B2-54, C2-25) (Figure S1H). These findings indicate that high levels of FGFR1 are expressed in

Figure 1. FGFR Signaling Promotes MB Cell Dissemination

(A) Spheroid invasion assay (SIA) with MB cell lines. Images of spheroids after 24 hr in the absence or presence of bFGF and distance of invasion from centers of spheroids are shown (n = 3 biological replicas; means ± SD).

(B) IHC images of low, moderate, and high expression of FGFR1 in MB TMA. Quantification of FGFR1 expression in MB TMA using H-scoring.

(C) SIA using DAOY, UW228, and Med311PDX cells stimulated with bFGF in the absence or presence of BGJ398 or in the absence or presence of CK666 for 24 hr. Drug concentrations are indicated in Figure S2A (n = 3 biological replicas; means ± SD).

(D) Confocal immunofluorescence analysis (IFA) of LA-EGFP-expressing DAOY cell spheroids in OCSCs cultured in the absence or presence of BGJ298 for 5 days and distance of tissue infiltration (pooled data from n = 4 biological replicas).

(E) Orthotopic G3 MB tumor-bearing mice were treated for 10 days with either solvent or BGJ398. Collapsed stacks of confocal microscopy sections of whole brains are shown. Yellow highlighted area shows tumor expansion in the brain tissue. (a) Area of tumor relative to the whole brain (n = 5 control, 4 treated). (b) GFP fluorescence in tumor areas (n = 5 control, 4 treated).

(F) Confocal microscopy sections of cortical cerebellum of three control and three BGJ398-treated mice. Inverted grayscale images of GFP fluorescence depict tumor masses and invading cells. Arrowheads indicate individual tumor cells in cerebellar tissue, and arrows indicate tumor cells migrating along cerebellar fissures. Stitched tile series acquired with 10x objective and 4x digital magnifications of boxed areas are shown. 4× magnifications of boxed areas are shown. (a) Dot plot of all infiltrating single cells analyzed in control and BGJ398-treated mice. (b) Comparison of average distance of infiltration of individual cells in five control and four BGJ398-treated mice. (c) Sum of all infiltration distances in five control and four BGJ398-treated mice.

(G) OCSC co-cultured with DAOY cell spheroid for 15 days in the presence of 100 ng/mL bFGF. (a) and (b) are 4× magnifications of boxed areas.

(H) Confocal z stack of a DAOY cell spheroid in the absence or presence of bFGF stimulation for 24 hr and magnifications of boxed areas (blue, Hoechst [nuclei]; green, LA-EGFP).

(I) Single confocal sections of anti-myosin-X staining in DAOY cells seeded on a thick layer of collagen in the absence or presence of bFGF for 18 hr. Yellow arrowheads indicate bFGF-induced filopodia-like protrusions.

(J) Single confocal sections of anti-myosin-X staining in DAOY spheroids embedded in collagen in the absence or presence of bFGF for 18 hr. Magnifications are 4× of boxed areas. Yellow arrowheads indicate filopodia-like protrusions.

*** $p \leq 0.001$), **** $p \leq 0.0001$. See also Figures S1 and S2.

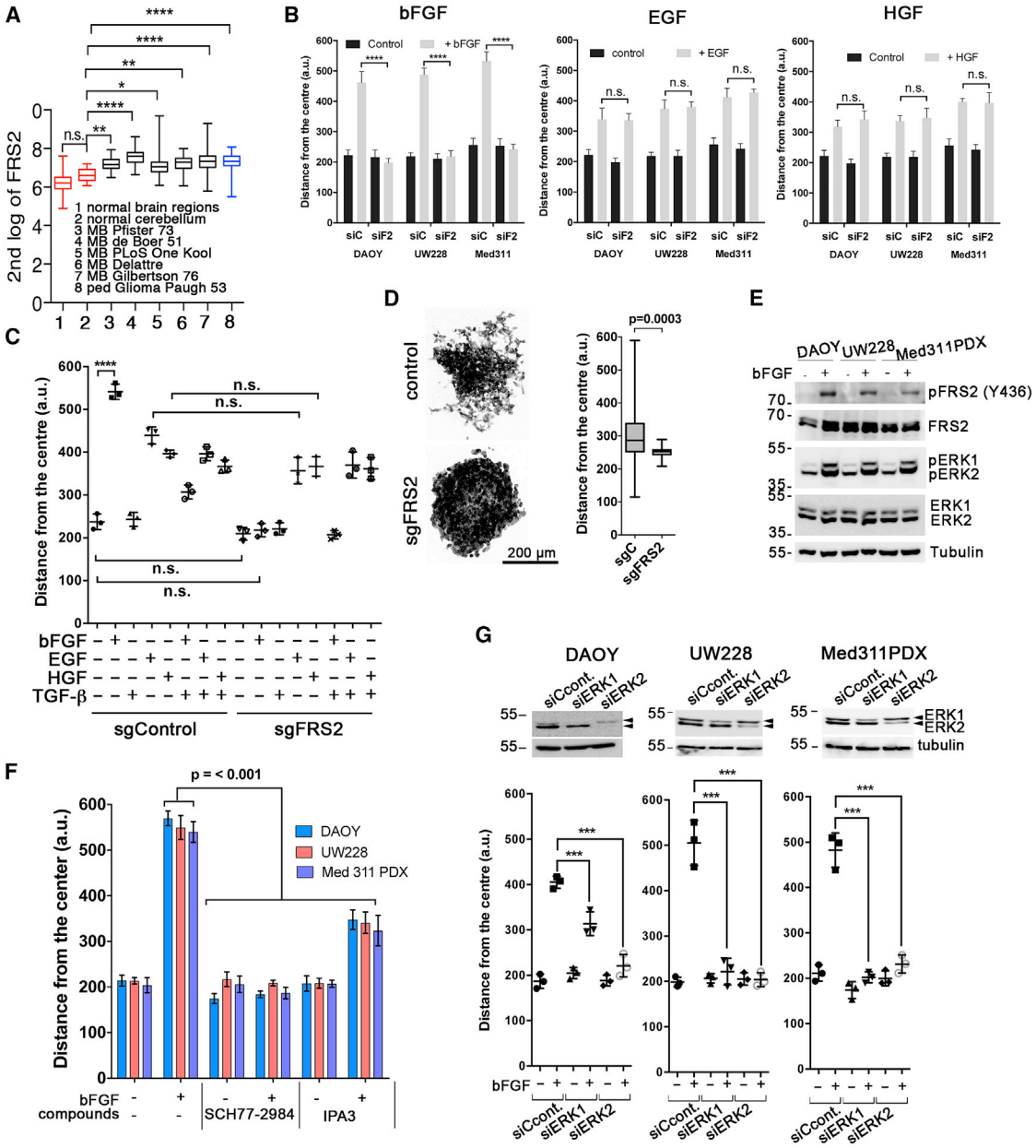

Figure 2. Pro-migratory FGFR Signaling Is Mediated through FRS2

(A) Microarray data analysis for FRS2 mRNA expression in healthy brain and tumor tissues.

(B) SIA using DAOY, UW228, and Med311PDX spheroids transfected with siControl or siFRS2 and treated with bFGF (100 ng/mL), EGF (30 ng/mL), or HGF (20 ng/mL) for 24 hr (n = 3 biological replicas; means ± SD).

(C) SIA using DAOY sgControl and DAOY sgFRS2 cells stimulated with bFGF, TGF-β, EGF, or HGF combinations for 24 hr (n = 3 biological replicas; means ± SD).

(D) Confocal IFA of LA-EGFP expressing sgControl or DAOY sgFRS2 cell spheroids in OCSCs after 5 days of co-culture. Distance of dissemination was determined using aCDc (pooled data from n = 4 biological replicas).

(E) Immunoblot (IB) of DAOY, UW228, and Med311PDX cell lysates after stimulation with bFGF for 10 min.

(F) SIA using DAOY, UW228, and Med311PDX cells stimulated with bFGF in the absence or presence of SCH772984 or in the absence or presence of IPA3 (n = 3 biological replicas; means ± SD).

(G) Upper: IB of DAOY, UW228, and Med311PDX cell lysates 48 hr after siMAPK3 (ERK1) or siMAPK1 (ERK2) transfection. Lower: SIA of DAOY, UW228, and Med311PDX cells transfected with siMAPK3 or siMAPK1 in the absence or presence of bFGF stimulation for 24 hr (n = 3 biological replicas; means ± SD).

* $p \leq 0.05$, ** $p \leq 0.01$, *** $p \leq 0.001$), **** $p \leq 0.0001$. See also Figures S2 and S3.

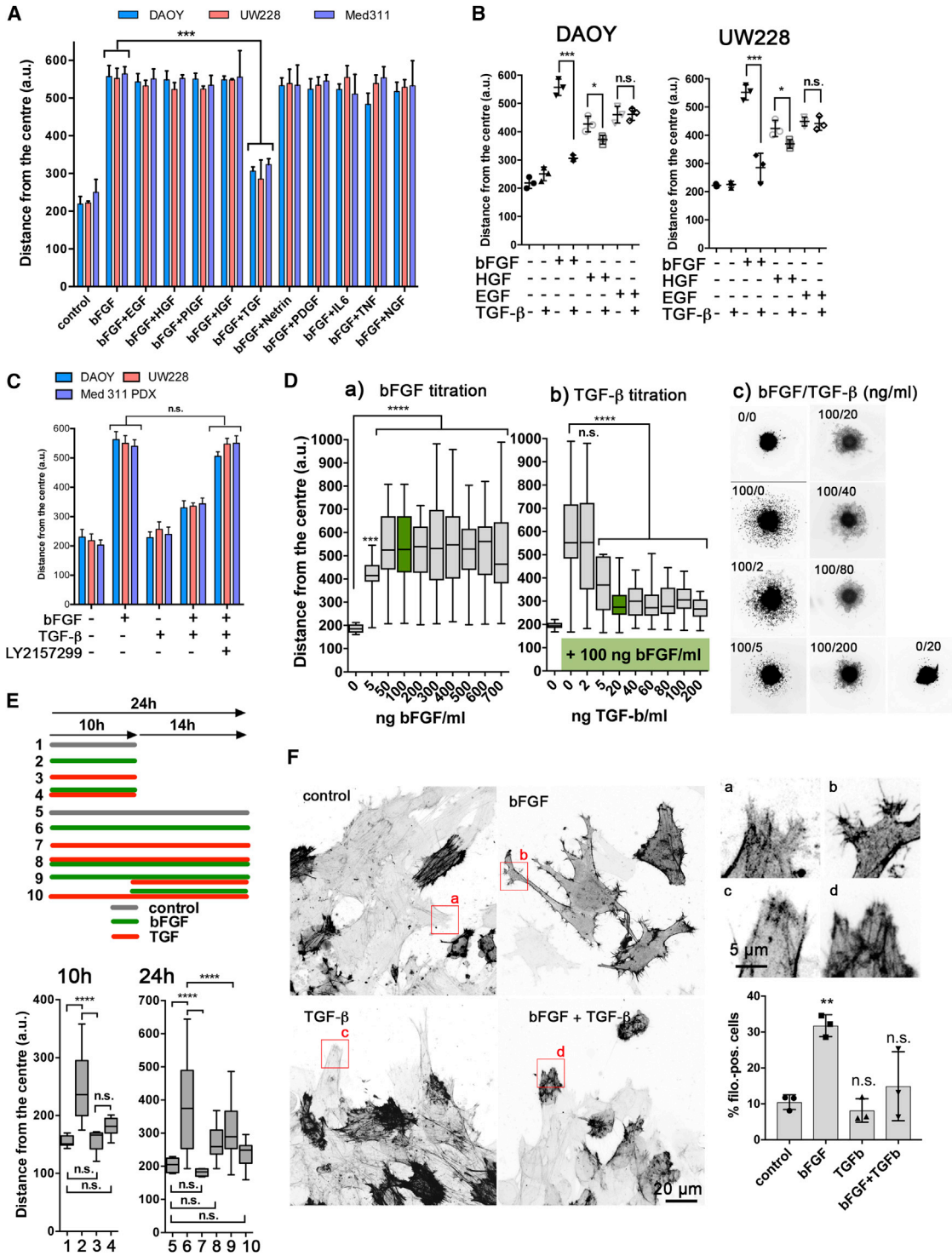

Figure 3. TGF-β Antagonizes bFGF-Induced Cell Invasiveness

(A) SIAs using growth factors at concentrations as described in STAR Methods in combination with bFGF (100 ng/mL) (n = 3 biological replicas; means ± SD).

(B) SIA using combinations of bFGF or EGF or HGF with TGF-β for 24 hr in DAOY and UW228 cells (n = 3 biological replicas; means ± SD).

(C) SIA of cells treated with bFGF plus TGF-β in the absence or presence of LY2157299 for 24 hr (n = 3 biological replicas; means ± SD).

(D) SIA (pooled data of n = 2 biological replicas) for (a) bFGF titration in DAOY cells and (b) TGF-β titration in bFGF-stimulated DAOY cells. Green labels highlight effective concentrations used in subsequent experiments. (c) Representative images of (b).

(legend continued on next page)

MB tumor cells and suggest that the source of bFGF *in vivo* is individual cells either residing in or infiltrating the tumor.

FGFR Signaling Promotes Collagen I and Tissue Invasion

To test the functional relevance of FGFRs, we used the pan-FGFR inhibitor BGJ398 (Guagnano et al., 2011), which reduced bFGF-induced collagen I invasion to basal levels at 5 μM (Figures 1C and S2B), a concentration not affecting cell viability (Figure S2C). bFGF treatment significantly increased the average velocity of collagen I invasion from 0.38 μm/min (untreated control) to 0.74 μm/min (Figure S2D). Mitomycin C, which completely abrogated cell proliferation 24 hr after treatment (Figure S2E), neither blocked collagen I invasion nor significantly reduced the number of invaded cells (Figure S2F), excluding the possibility that proliferation contributes to increased cell dispersal after bFGF stimulation. BGJ398 treatment of organotypic cerebellum slice cultures (OCSCs) (Neve et al., 2017) blocked brain tissue infiltration of co-cultured DAOY tumor spheroids (Figure 1D), indicating that FGFR activity is necessary for cell dissemination *ex vivo*. We next explored the significance of FGFR signaling for MB progression using a GFP-expressing group 3 MB orthotopic mouse model (Pei et al., 2016). We found that orally administered BGJ398 for 10 days in tumor-bearing mice reduced tumor expansion and total GFP fluorescence compared to solvent-treated control mice (Figures 1Ea and 1Eb). Importantly, FGFR inhibition also significantly reduced the total number of cells infiltrating the parenchyma as well as individual and cumulated infiltration distances (Figures 1Fa–Fc). The dissemination of tumor cells along the fissures (arrows in Figure 1F) was not affected in the BGJ398-treated animals.

Cells infiltrating the cerebellum in OCSCs displayed F-actin-rich, filopodia-like invasive protrusions (Neve et al., 2017) (Figure 1G). These resemble the highly dynamic lamellipodia- and filopodia-like structures at the leading edge of collagen I-invading MB cells (Figure 1H; Video S1), which characterize mesenchymal motility and invading cancer cells (Jacquemet et al., 2015, 2017). Inhibition of F-actin polymerization in lamellipodia and filopodia (Korobova and Svitkina, 2008; Suraneni et al., 2012) using the Arp2/3 complex inhibitor CK666 (Hetrick et al., 2013), abrogated bFGF-induced dissemination (Figure 1C). We detected the actin-based motor protein myosin-X (Kerber and Cheney, 2011; Lai et al., 2015) at the tip of filopodia-like protrusions, both in cells seeded on a collagen layer (Figure 1I) and embedded in collagen I (Figure 1J), and vasodilator-stimulated phosphoprotein (VASP) at the base and in the shaft of the protrusions (Figure S2G). Thus, bFGF triggers FGFR-driven mesenchymal motility and invasiveness that is dependent on F-actin polymerization and associated with the formation of lamellipodia- and filopodia-like protrusions.

FRS2 Is Required for FGFR-Driven Invasion

FGFRs signal through the adaptor protein FRS2 (Turner and Grose, 2010). We detected high FRS2 mRNA levels in human MB tissue samples compared to normal brain regions, including cerebellum (Figure 2A), and detectable levels in all sub-groups of established MB and PDX cell lines tested (Figure S2H). The depletion of FRS2 by small interfering RNA (siRNA) (Figure S2I) specifically abrogated bFGF-induced collagen I invasion (Figure 2B). Consistently, the knockdown of FRS2 using CRISPR/Cas9 (Figure S2J) prevented collagen I invasion *in vitro* (Figure 2C) and the infiltration of cerebellum in OCSCs *ex vivo* (Figure 2D). Stimulation of cells with bFGF also increased phosphorylation of FRS2 and of ERK1/2 (Figure 2E). Pharmacological inhibition of ERK with SCH77-2984 (Figure 2F) or depletion of ERK1 or ERK2 using siRNA significantly reduced bFGF-induced collagen I invasion (Figure 2G). The same treatments only minimally affected epidermal growth factor (EGF)- and hepatocyte growth factor (HGF)-induced collagen I invasion (Figure S3A). Inhibitor against other FGFR effectors such as PKC, PI3-K, or JNK did not prevent bFGF-induced collagen I invasion (Figures S3B and S3C), except for PAK-1 (Figure 2F), but blocked collagen I invasion induced by EGF or HGF (Figure S3D). Thus, MB tumor cells depend on FRS2 and signaling through ERK1/2 and PAK for FGFR-driven invasion.

TGF-β Signaling Antagonizes bFGF-Induced Cell Invasion

Using collagen I invasion as a readout, we determined the concentrations necessary for minimal and maximal significant invasion induced by a panel of 11 growth factors or cytokines (Figures S4A and S4B). These high and low concentrations allowed us to explore synergistic and antagonistic effects of factor combinations on collagen I invasion using a Plackett Burman (PB) screening matrix (Figure S4C). We detected no additive or synergistic effects (Figure S4D), but found that TGF-β specifically abrogated cell migration induced by bFGF (Figures 3A and 3B). The inhibition of the TGF-β receptor (TβR) activities with LY2157299 rescued bFGF-induced migration in co-stimulated cells in a dose-dependent manner (Figures 3C and S4E). By testing a range of different bFGF and TGF-β concentrations, we found that at least 20 ng/mL TGF-β was required to effectively block bFGF-induced migration and that concentrations above 20 ng/mL TGF-β did not increase the antagonistic effect (Figure 3D). The blockade of bFGF-induced collagen I invasion by TGF-β was immediate, as it mitigated bFGF function even after 10 hr pre-treatment with bFGF (Figure 3E). TGF-β treatment did not cause the formation of filopodia-like protrusions (Figure S4F), and TGF-β co-stimulation reduced the number of filopodia-like protrusions compared to cells stimulated with bFGF alone (Figure 3F). These data identified the TGF-β pathway as a repressor of pro-invasive bFGF-FGFR signaling in MB cells.

Relative Levels of bFGF and TGF-β Determine Invasive Behavior

To explore whether exposure to bFGF or TGF-β affected tumor cell dissemination, we assessed the impact of exogenous

(E) Top: Treatment schemes for SIA using DAOY cells with bFGF or TGF-β treatment for 10 hr followed by co-stimulation with bFGF and TGF-β for 14 hr. Bottom: Quantification of resulting SIAs (n = 2 biological replicas).

(F) Left: Confocal IFA images of control and stimulated DAOY-LA-EGFP cells migrating from collagen I embedded spheroids. Top right: (a)–(d) are 4× magnifications of boxed areas. Bottom right: Quantification of percentage of cells displaying filopodia-like protrusions (n = 3 biological replicas; means ± SD).

* $p \leq 0.05$, ** $p \leq 0.01$, *** $p \leq 0.001$), **** $p \leq 0.0001$. See also Figure S4.

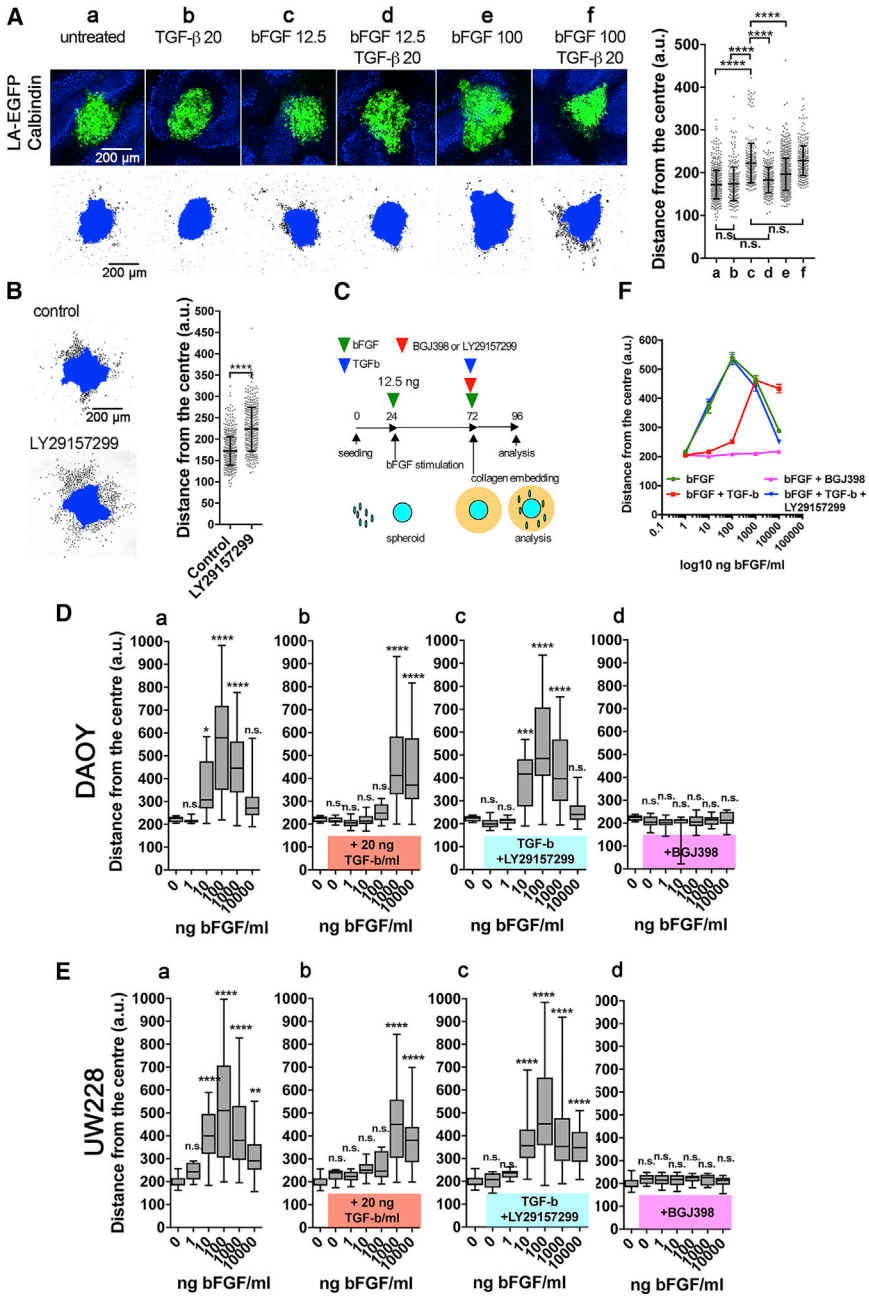

Figure 4. TGF-β Rescues Migration under High bFGF Conditions

(A) Upper row: Confocal IFA images of OCSCs and DAOY spheroids co-culture for 5 days in the absence or presence of the factors indicated. Concentrations indicated as nanograms per milliliter. Blue: Calbindin; green: LA-EGFP. Lower row: Quantification of single-cell infiltration. Blue area indicates non-infiltrated tumor cell mass. Black dots are nuclei of infiltrated cells. Distance of invasion from center of tumor mass is shown in dot plot on the right (n = 6 spheroids/condition from two biological replicas; mean ± SD).

(B) Quantification of single-cell infiltration as described in (A) for control and OCSCs-treated with 5 μM LY29157299 (n = 6 spheroids/condition from two biological replicas; mean ± SD).

(C) Schema of experimental setup for SIA quantified in (D) and (E) with 36-hr pre-treatment with 12.5 ng/mL bFGF.

(D and E) SIA using DAOY (D) and UW228 (E) cells after pre-treatment with bFGF as indicated in (C). bFGF dose-response in the absence or presence of 20 ng/mL TGF-β in combination with BGJ398 or LY29157299 (pooled data from n = 2 biological replicas).

(F) x/y line graph of means and SEMs of (D).

* $p \leq 0.05$, ** $p \leq 0.01$, *** $p \leq 0.001$), **** $p \leq 0.0001$. See also Figure S5.

bFGF and TGF-β on cell infiltration in OCSCs. We observed that MB cells disseminated from spheroids implanted in OCSCs in the absence and under conditions of 12.5 ng/mL exogenous bFGF (Figures 4Aa and 4Ac). TGF-β treatment caused spheroid compaction in the absence of exogenous bFGF and reduced cell infiltration in the presence of 12.5 ng/mL exogenous bFGF (Figures 4Ab and 4Ad). Increasing exogenous bFGF to 100 ng/mL reduced invasion compared to treatment with 12.5 ng/mL bFGF (Figures 4Ac and 4Ae). Interestingly, addition of TGF-β in the presence of 100 ng/mL bFGF increased cell infiltration compared to stimulation with 100 ng/mL bFGF alone (Figures 4Ae and 4Af). Treatment of OCSCs with the TβR inhibitor LY29157299 also promoted tumor cell infiltration, indicating that TβR signaling repressed pro-invasive activities of the tumor cells in the OCSCs (Figure 4B). We hypothesized that (1) increasing bFGF concentrations above a certain threshold might constrain the pro-invasive activity of bFGF and (2) parallel exposure to TGF-β could rescue invasion. If true, bFGF should be present endogenously in the OCSCs and ectopic addition of bFGF could raise total bFGF levels over and above such a suspected threshold. Consistent with this possibility, bFGF was detected in the slices (Figure S5A) and around the implanted tumor spheroids by immunofluorescence analysis (IFA) (Figure S5B). Therefore, we compared collagen I invasion at increasing bFGF concentrations to determine the pro-invasive dose response of bFGF *in vitro*. To simulate the *ex vivo* conditions of prolonged bFGF exposure in OCSCs, we pre-treated the cells with 12.5 ng/mL bFGF for 48 hr (Figure 4C). We found that invasiveness diminished at concentrations above 100 ng/mL bFGF and that TGF-β blocked bFGF-induced dissemination up to 100 ng/mL bFGF (Figures 4D, 4Ea, 4Eb, and S5C); in the presence of very high concentrations of bFGF (10 μg/mL), however, TGF-β partially rescued migration and invasion (Figures 4D, 4Eb, and S5D). Blocking TβR with LY215729 deterred this TGF-β restoration of bFGF-induced invasion (Figures 4D and 4Ec), whereas BGJ398

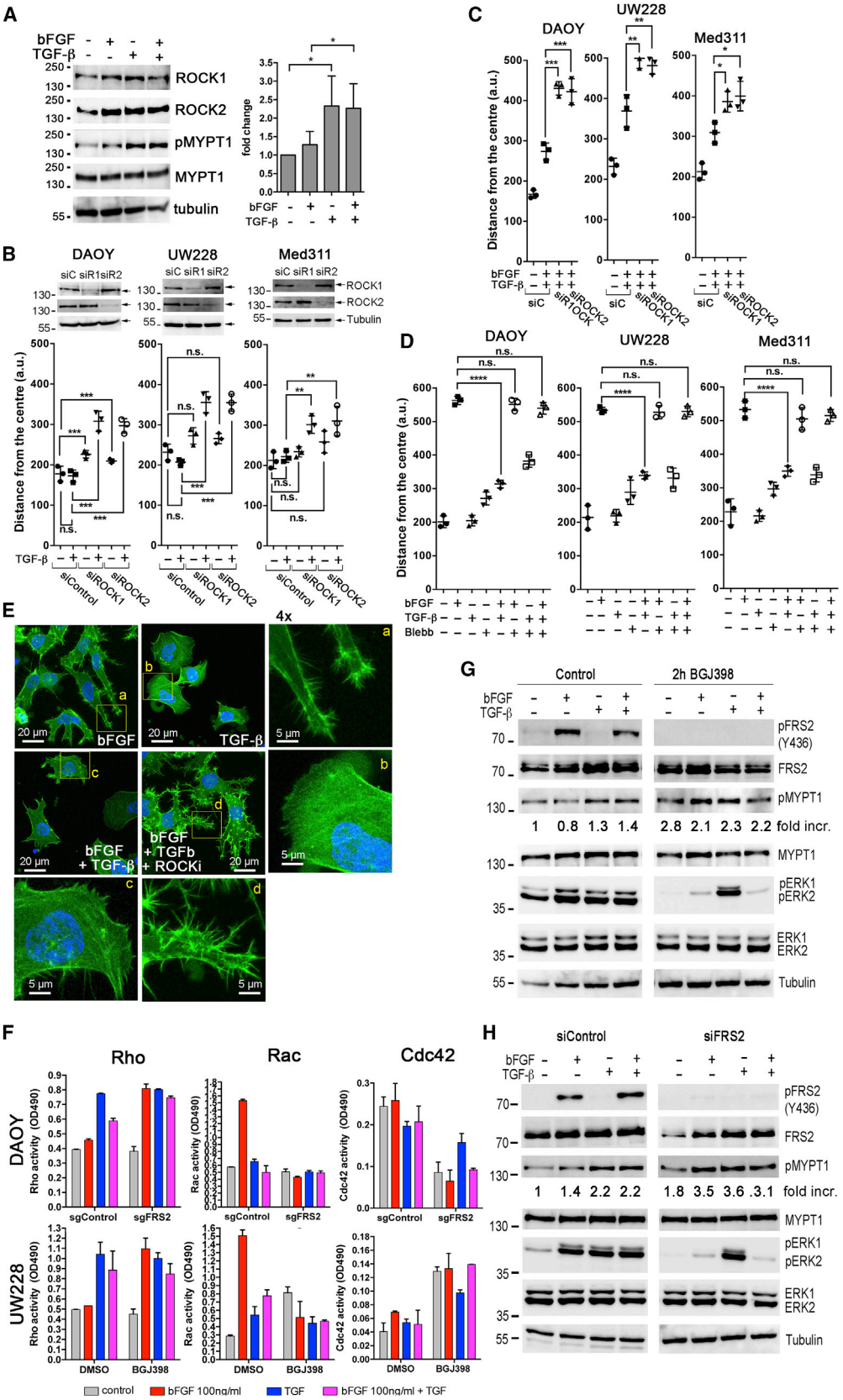

(legend on next page)

treatment prevented invasion at all bFGF concentrations (Figures 4D and 4Ed). A 5-day exposure to bFGF (100 ng/mL) and TGF-β (20 ng/mL) had no effect on tumor cell viability and proliferation (Figures S5E–S5H). bFGF concentrations higher than 100 ng/mL gradually reduced the metabolic activity of DAOY cells if applied for more than 48 hr (Figures S5E and S5F). The viability of Med311PDX remained unaltered at all concentrations of bFGF and TGF-β (Figures S5G and S5H). In conclusion, we found that TGF-β signaling antagonized collagen I invasion of MB cells at low bFGF concentrations and rescued invasion repressed by high levels of bFGF (Figure 4F).

Contractility Induced by TGF-β-ROCK Signaling Impairs Collagen I Invasion

In light of the possible balancing function of TGF-β, we explored its expression in MB tumor cells and tissues. qRT-PCR revealed variable levels of TGF-β in MB cell lines (Figure S6A), and by IHC we observed TGF-β-expressing cells accumulating in the vascularized regions of MB tissues, which otherwise were devoid of anti-TGF-β staining (Figure S6B). MB cells and tumor tissues predominantly express TβR II and to a lesser extent TβR I (Figures S6A, S6C, and S6D). Non-canonical TβR signaling can induce a contractile phenotype through the Rho-associated kinase ROCK (Maddox and Burridge, 2003; Zhang, 2009). Exposing MB cells to TGF-β increased the phosphorylation of the ROCK substrate myosin phosphatase target subunit 1 (MYPT1) (Figures 5A and S6E). Depletion of ROCK using siRNA or inhibition with Y27632 increased collagen I invasion and converted TGF-β into a pro-migratory factor (Figures 5B and S6F). Depletion of ROCK1/2 or its inhibition—but not inhibition of ERK1/2 or PAK—rescued collagen I invasion in cells co-stimulated with bFGF and TGF-β (Figures 5C and S6G). Inhibition of myosin II with blebbistatin rescued bFGF-induced collagen I invasion in the presence of TGF-β, suggesting that contractility is necessary for TGF-β-dependent repression of bFGF signaling (Figure 5D). TGF-β treatment of collagen I-embedded cells caused contracted, rounded cell phenotypes (Figure 5E; Video S2), and the inhibition of ROCK triggered formation of filopodia-like protrusions (Figure 5E). TGF-β stimulation increased the activity of the Rho family GTPases Ras homolog A (RhoA), whereas it left Ras-related C3 botulinum substrate 1 (Rac1) activity unaltered (Figure 5F). FGFR inhibition (Figure 5G) or FRS2 depletion (Figure 5H) increased phosphorylation of MYPT1, which was further increased in cells co-stimulated with bFGF and TGF-β (Figures 5G, 5H, and S6H). This suggested that FGFR1-FRS2 signaling repressed ROCK activation in the absence of TGF-β. Consistently, bFGF stimulation increased Rac1 but not RhoA activity in collagen I-embedded cells (Figure 5F). Conversely, TGF-β abrogated bFGF-induced Rac1 activation, indicating that TGF-β interferes with FGFR signaling upstream of Rac (Figure 5F). Preventing bFGF signaling by FRS2 depletion or FGFR inhibition increased RhoA in bFGF-stimulated cells (Figure 5F), corroborating the inhibitory effect of FRS2 on ROCK activity. Although the activity of cell division cycle 42 (Cdc42) was reduced in FRS2-depleted cells, its activity was not affected by bFGF stimulation (Figure 5F). Taken together, these data demonstrate that bFGF and TGF-β signaling antagonistically control Rac and Rho GTPases and that TGF-β triggers ROCK activation and cell contractility.

Activation of ERK1/2 by TGF-β Attenuates bFGF-Dependent Invasion at Low bFGF Abundance

A negative regulator of FRS2 function is ERK1/2, which acts by decreasing FRS2 tyrosine phosphorylation (Zhou et al., 2009). Both bFGF (Figure 2E) and TGF-β (Figure 6A) increased ERK1/2 activity, although with different kinetics (Figures 7B, S7A, and S7B). MB cells co-stimulated with bFGF and TGF-β displayed significantly lower tyrosine phosphorylation of FRS2 compared to cells stimulated with bFGF alone (Figures 6B and 6C). In these co-stimulated cells, inhibition of ERK1/2 with SCH772984 restored phosphorylation of FRS2 (Figures 6B and 6C). In contrast, inhibition of ERK1/2 in bFGF-stimulated cells did not increase FRS2 phosphorylation. Blebbistatin treatment also partially rescued the phosphorylation of FRS2 (Figure 6D), suggesting that the contractile phenotype induced by TGF-β is necessary for ERK1/2-dependent FRS2 repression. To distinguish bFGF-activated from TGF-β-activated ERK1/2 and to decipher the relationship between contractility and ERK1/2 activation, we tested whether TGF-β-induced contractility influenced the activation and localization of ERK1/2. We found that blebbistatin treatment prevented TGF-β activation of ERK1/2 without affecting bFGF-activated ERK1/2 (Figures 6E and 6F). This signified that TGF-β-induced pERK1/2 was dependent on contractility. Stimulation of cells with bFGF caused cytosolic localization of pERK1/2 (Figure 6G). In contrast, stimulation of cells with TGF-β or with bFGF and TGF-β caused the localization of a fraction of pERK1/2 to the plasma membrane (Figures 6G and 6H). This finding suggested that TGF-β induced contractility spatially oriented active ERK1/2 in close proximity to FRS2 (near plasma membrane), leading to ERK1/2-dependent inactivation

Figure 5. TGF-β Causes ROCK Activation and Represses the Formation of Filopodia-Like Protrusions

(A) Left: IB of DAOY cell lysates after stimulations as indicated for 10 min. Right: Quantification of fold change of pMYPT1 (n = 3 biological replicas; means ± SD).
(B) Upper: IB of cell lysates 48 hr after siROCK1 or siROCK2 transfection. Lower: SIA comparing cells transfected with siROCK1 or siROCK2, in the absence or presence of TGF-β stimulation for 24 hr (n = 3 biological replicas; means ± SD).
(C) Same as (B) except that cells were also treated with bFGF.
(D) SIA of cells treated with TGF-β in the absence or presence of blebbistatin for 24 hr (n = 3 biological replicas; means ± SD).
(E) Collapsed confocal z stacks of SIA of DAOY LA-EGFP cells treated as indicated for 24 hr.
(F) Active Rho, Rac, and Cdc42 GTPase ELISA assay in sgControl, sgFRS2, and UW228 cells embedded in collagen I in the absence or presence of BGJ398 and following stimulation with bFGF, TGF-β, or bFGF plus TGF-β for 24 hr (n = 3 biological replicas; means ± SD).
(G) IB of DAOY cell lysates in the absence or presence of BGJ398 and after stimulation with bFGF, TGF-β, or bFGF plus TGF-β for 10 min. Fold change of pMYPT1 is indicated below the pMYPT1 panels.
(H) IB of DAOY cell lysates after transfection with non-targeted siRNA (siControl) or siFRS2 and after 10 min stimulation with indicated factors.
* $p \leq 0.05$, ** $p \leq 0.01$, *** $p \leq 0.001$), **** $p \leq 0.0001$. See also Figure S6.

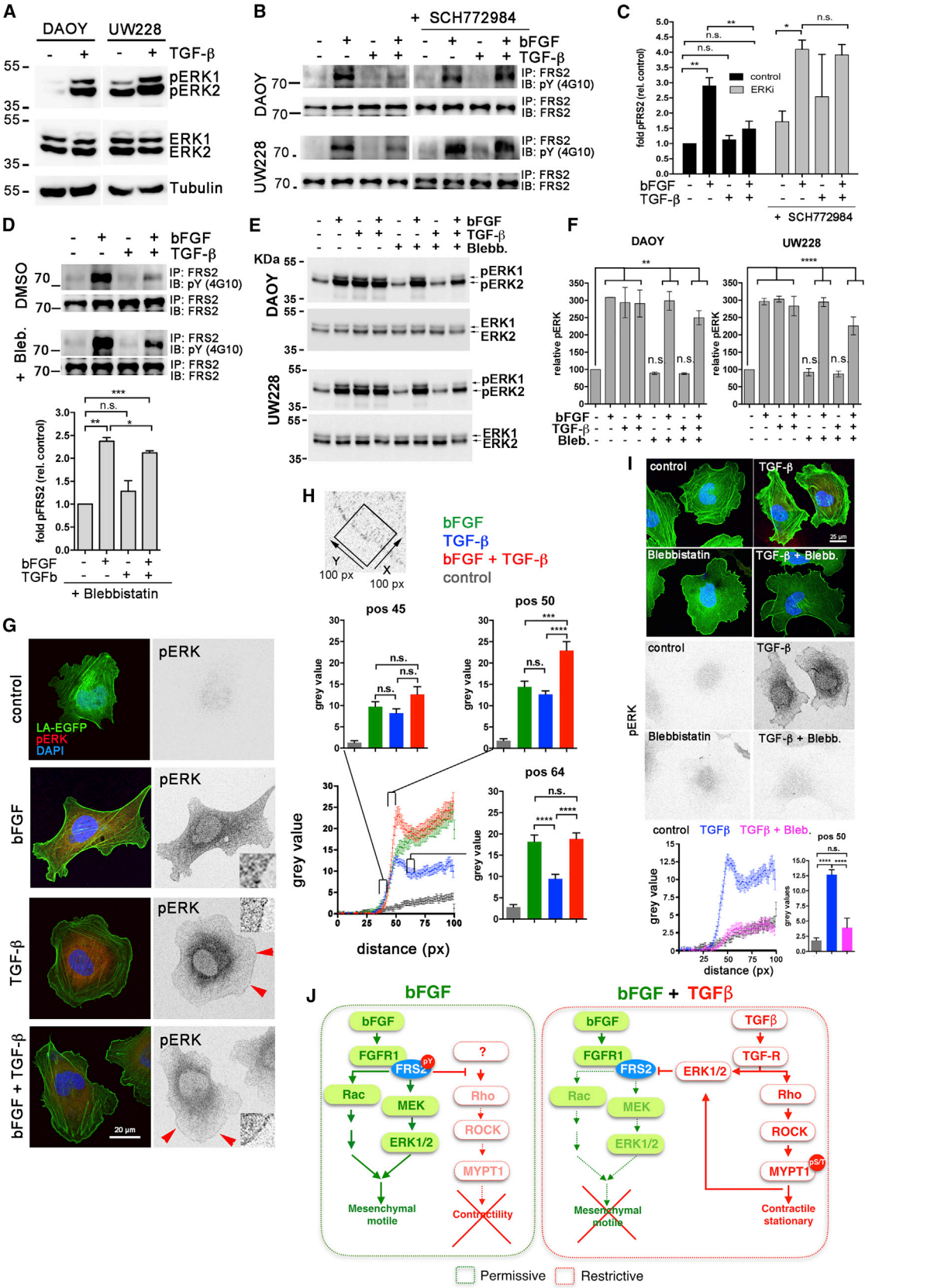

(legend on next page)

of FRS2. Consistently, blocking contractility with blebbistatin completely abrogated the plasma membrane localization of pERK1/2 (Figure 6I). Taken together, co-incidence of activated ERK1/2 and contractility are required for the effective mitigation of FRS2 activity by TGF-β (Figure 6J).

TGF-β Impairs Negative-Feedback Regulation of FRS2 at High bFGF Abundance and Rescues Invasion

Stimulation of MB cells with 100 ng/mL bFGF caused a 2- to 3-fold increase in pFRS2, which was sustained for 24 hr (Figures 6C and 7B). 10 μg/mL bFGF applied for 24 hr caused only marginal Tyr phosphorylation of FRS2 (Figure 7A). ERK1/2 inhibition with SCH772984 or co-stimulation with TGF-β restored FRS2 phosphorylation in MB cells stimulated with 10 μg/mL bFGF (Figure 7A). To test whether this variable FRS2 activation resulted in a corresponding signaling response, we monitored the dynamics of ERK1/2 activation in cells exposed to either 100 ng/mL or 10 μg/mL bFGF. We found that 100 ng/mL bFGF caused sustained ERK1/2 activation for 24 hr. In contrast, 10 μg/mL bFGF caused peak activation of ERK1/2 for 60 min, followed by a drop to basal levels (Figures 7B, S7A, and S7B). 10 μg/mL bFGF also caused transient FRS2 phosphorylation for 60 min followed by gradual inactivation within 24 hr (Figure 7C). This gradual inactivation of FRS2 was prevented in the presence of SCH772984 (Figure 7C), suggesting that the ERK1/2-induced inhibition occurs at or upstream of FRS2. Stimulation with TGF-β led to a bi-phasic activation of ERK1/2, a signature also found in cells co-stimulated with 100 ng/mL bFGF (Figures 7B, S7A, and S7B). Interestingly, impaired sustained activation of ERK1/2 at 10 μg/mL bFGF was restored by TGF-β within 60 min, confirming that TGF-β reverts the negative-feedback inhibition of bFGF signaling (Figure 7B). TGF-β restoration of pFRS2 at high bFGF was independent of ERK1/2 (Figure 7A), and it was also independent of ROCK, as we neither detected phosphorylation of MYPT1 in 10 μg/mL bFGF plus TGF-β (Figures 7D and S7C) nor increased RhoA (Figure 7E). However, and in contrast to bFGF 100 ng/mL plus TGF-β, Rac1 activity remained high in bFGF 10 μg/mL plus TGF-β (Figure 7E). Thus, in the context of high bFGF levels, FGFR signaling is self-inhibited by ERK1/2 through negative feedback. This negative feedback is dampened by TGF-β, which maintains FRS2 in the active state to repress ROCK and to promote MB cell dissemination through Rac1 (Figure 7F).

DISCUSSION

Our study shows that bFGF-expressing cells populate the MB tumor microenvironment and that impairing FGFR signaling prevents tissue infiltration of tumor cells promoted by the adaptor protein FRS2. In the context of low bFGF levels, non-canonical TGF-β signaling restricts pro-invasive functions of FGFR by repressing FRS2 phosphorylation. FRS2 repression involves cortical accumulation of activated ERK1/2, which is the result of TGF-β-dependent simultaneous induction of ERK1/2 activity and ROCK-mediated contractility. In the context of high bFGF levels, which causes ERK1/2-dependent negative-feedback inhibition of FGFR signaling, TGF-β rescues invasion by impairing negative-feedback regulation of FGFR and restoring FRS2 phosphorylation. The molecular integrator of the rheostat regulation of FGFR function by TGF-β is FRS2, pinpointing it as a critical coordinator of the invasive outcome of MB cells exposed to variably abundant bFGF and TGF-β in the brain microenvironment.

We found that bFGF-FGFR signaling potently triggers pro-invasive cell functions in MB, similar to mesenchymal cellular characteristics (Friedl and Wolf, 2010). TGF-β signaling restricts these mesenchymal characteristics through the activation of RhoA-ROCK and concomitant repression of FRS2 tyrosine phosphorylation by ERK1/2. Repression of FRS2 tyrosine phosphorylation by ERK1/2 was previously described for EGF, platelet-derived growth factor (PDGF), and insulin-like growth factor (IGF) signaling through phosphorylation of inhibitory threonine residues on FRS2 (Gotoh, 2008; Zhou et al., 2009). Our data demonstrate that TGF-β can analogously inhibit FRS2 and prevent pathological cell mobilization under the condition of low bFGF abundance.

ROCK activation in mesenchymal cells causes cortical contractions and cell rounding (Nobes and Hall, 1999). Tumor cells exploit this cellular plasticity and adopt different motility modes during tissue invasion (Sahai and Marshall, 2003; Torka et al.,

Figure 6. TGF-β-Induced ERK Represses FRS2 Activation

(A) IB of DAOY and UW228 cell lysates after stimulation with TGF-β for 10 min.

(B) DAOY and UW228 cells treated in the absence or presence of SCH772984 for 4 hr followed by stimulation with bFGF, TGF-β, or co-stimulation with bFGF and TGF-β for 10 min were subjected to immunoprecipitation (IP) anti-FRS2 followed by IB anti-pTyr.

(C) Integrated density of pFRS2 bands of (B) relative to unstimulated control (n = 3 biological replicas; means ± SD).

(D) Same as (B), except the cells were treated in the absence or presence of blebbistatin (n = 3 biological replicas; means ± SD).

(E) IB of cells treated in the absence or presence of blebbistatin for 4 hr followed by stimulation with bFGF, TGF-β, or co-stimulation with bFGF and TGF-β for 10 min.

(F) Quantification of pERK in (E) (n = 3 biological replicas; means ± SD).

(G) Confocal IFA images of pERK in DAOY cells on collagen-coated plates in the absence or presence of bFGF, TGF-β, or bFGF plus TGF-β for 24 hr.

(H) Quantification of cumulated gray values across cell margins. Average and SEM are plotted as xy graphs (lower left, n = 2 biological replicas; cells/fields/measurements: control, 20/10/34; bFGF, 29/15/54; TGF-β, 19/14/43; bFGF plus TGF-β, 34/16/65). Average and SEM of regions on and behind cell margins as indicated on the xy plot are shown in the column diagrams.

(I) Confocal IFA images of TGF-β-treated cells in the absence or presence of blebbistatin. Quantification of pERK distribution across cell margins as described in H. n = 2 biological replicas; cells/fields/measurements: control, 20/10/34; TGF-β, 19/14/43; TGF-β plus blebbistatin, 22/8/27.

(J) Schematic representation of (left) the inhibition of ROCK by FRS2 in the absence of TGF-β and (right) the inhibition of FRS2 by TGF-β induced ERK and ROCK-dependent contractility.

* $p \leq 0.05$, ** $p \leq 0.01$, *** $p \leq 0.001$), **** $p \leq 0.0001$.

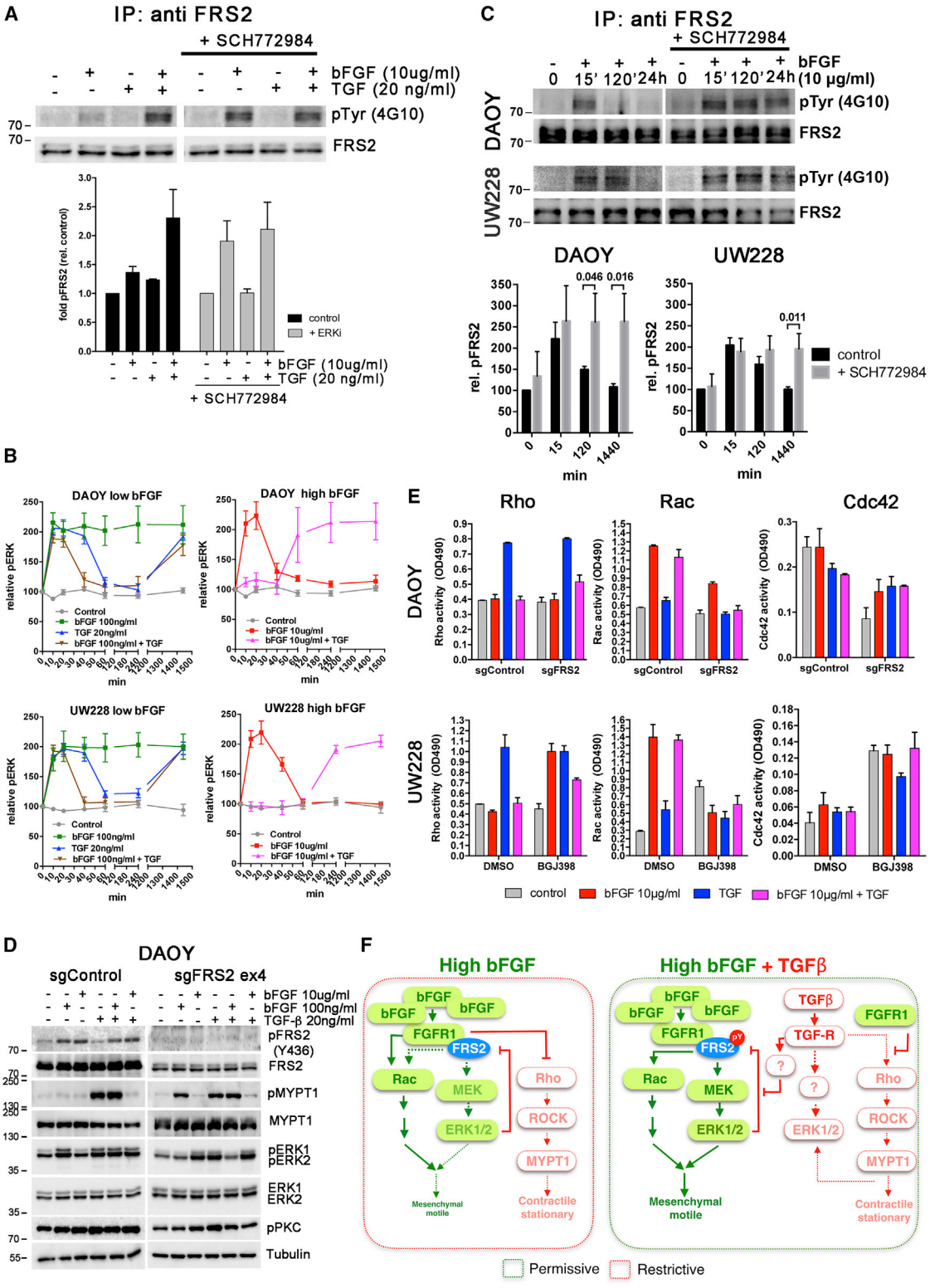

Figure 7. TGF-β Reverts Negative-Feedback Regulation of FRS2 under High bFGF

(A) IP anti-FRS2 followed by IB anti-total pY in DAOY cells. Stimulations as indicated for 24 hr. Bar graph shows fold change of FRS2 phosphorylation relative to untreated control (n = 3 biological replicas; means ± SD).

(legend continued on next page)

2006). We propose that, in the absence of TGF-β, FGFR-FRS2 signaling reprograms the cytoskeleton toward mesenchymal migration by maintaining a state of moderate ROCK repression, which promotes the formation of filopodia-like protrusions for tissue invasion (Jacquemet et al., 2015). In the presence of TGF-β, the moderate repression of ROCK by FRS2 is overpowered by non-canonical TGF-β signaling, resulting in a more contractile phenotype and in the cortical activation of ERK1/2. Our findings furthermore indicate that ROCK activation promotes cortical translocation of ERK1/2 and that spatial re-localization of ERK1/2 is necessary for its inhibitory function on FRS2. Similar to our findings, ROCK-induced repression of motility and invasiveness observed in various other cancers (Adachi et al., 2011; Wei et al., 2016; Yang and Kim, 2014) could be due to its impact on spatial control of ERK1/2 activity in the tumor cells.

Sustained ERK1/2 activation at low abundance of bFGF is antagonized by TGF-β, causing bi-phasic ERK1/2 activation similar to TGF-β treatment alone. This suggests that sustained FGFR pathway activation is necessary for bFGF-induced pro-migratory signaling in the tumor cells. Peak activation of ERK1/2 in response to high bFGF abundance consistently inactivates FRS2 by negative feedback and halts pro-migratory signaling. FRS2 inactivation is reverted both by parallel TGF-β stimulation or ERK1/2 repression, indicating that TGF-β impacts ERK1/2-dependent negative-feedback regulation of FGFR signaling by a mechanism independent of RhoA-ROCK and ERK1/2.

Variably abundant growth factors and cytokines within the tumor and surrounding stroma result in graded exposure to these factors (Thoma et al., 2014). bFGF-positive cells within the MB tumor microenvironment could be indicative of uniform bFGF exposure with steep gradients at locations where bFGF-producing cells accumulate. MB cells display a biphasic dose-response to bFGF as bFGF is pro-migratory between 5 and 100 ng/mL and becomes anti-migratory above 100 ng/mL. The response to TGF-β is sigmoid, whereby any concentration above 20 ng/mL TGF-β confers the same outcome. Thus, TGF-β may provide a pro-migratory environment within tumor regions with very high bFGF levels. This effect may guide responsive tumor cells toward low bFGF abundance, where TGF-β restricts migration. This would suggest a context-dependent functionality of TGF-β (Massagué, 2012) regulating pro-invasive functions in MB. TGF-β-positive cells are present specifically in vascularized regions of MB tumor tissue. Hence, cross talk with bFGF signaling could contribute, along with bFGF co-factors such as sulfation patterns and the length of heparin sulfate chains (Matsuo and Kimura-Yoshida, 2013), to the modulation of the pro-migratory response in these critical zones (Figure S7D).

A recent study found that bFGF blockade of SHH activation prevents MB outgrowth, supporting the notion of activating FGF signaling for targeting SHH MB (Emmenegger et al., 2013). Our data indicate that caution is merited, since effective bFGF concentrations and the cross talk with TGF-β signaling described herein could increase tumor dissemination. Independent of bFGF concentration and the absence or presence of TGF-β, we identified FRS2 as the sole factor determining whether MB cells migrate and invade the bFGF-positive tumor microenvironment. Thus, FRS2 acts as a molecular hub for pro-invasive FGF signaling in MB, which renders it as an attractive target for anti-dissemination therapy.

STAR★METHODS

Detailed methods are provided in the online version of this paper and include the following:

- KEY RESOURCES TABLE
- CONTACT FOR REAGENT AND RESOURCE SHARING
- EXPERIMENTAL MODEL AND SUBJECT DETAILS
  - Human Subjects
  - Mouse Maintenance
- TISSUE CULTURE CELLS
  - Human MB Cell Lines
  - Patient-Derived Xenograft (PDX) Cell Culture
- METHODS DETAILS
  - Inhibitors
  - Spheroid Invasion Assay (SIA) and Automated Cell Dissemination Counter (aCDc)
  - Expression Analysis Using R2 Database
  - FRS2 Depletion by LentiCRISPR
  - Cell Proliferation WST-1 Assay
  - G-LISA
  - G-LISA—3D, IB
  - Growth Factor Treatments
  - In Vivo Experiments and Imaging
  - Confocal Immunofluorescence Analysis (IFA)
  - Confocal Live-Cell Imaging—SIA
  - Immunoblotting (IB)
  - Immunohistochemistry (IHC)
  - Immunoprecipitation
  - Organotypic Cerebellar Slice Culture
  - PB Design
  - RNA Expression Analysis by qRT-PCR
  - RNA Interference
- QUANTIFICATION AND STATISTICAL ANALYSIS

(B) Time course of pERK activation. Relative pERK was determined based on IB. Representative IBs and statistics are shown in Figures S7A and S7B (n = 3 biological replicas ± SEM).
(C) IP anti-FRS2 followed by IB anti-total pY. Bar graph shows FRS2 phosphorylation relative to total FRS2. p values of t test are indicated where $p \leq 0.05$ (n = 3 biological replicas; means ± SD).
(D) IB of cell lysates of collagen-embedded DAOY sgControl and DAOY sgFRS2 cells after stimulations as indicated for 24 hr.
(E) Active Rho, Rac, and Cdc42 GTPase ELISA using the cell lysates of DAOY cells described in (D) or UW228 (IB in Figure S7C) cells treated identically except for in the absence or presence of BGJ398 treatment (n = 3 biological replicas; means ± SD).
(F) Schematic representation of ERK1/2-induced negative-feedback inhibition of FRS2 and of TGF-β-mediated repression of negative-feedback inhibition at high levels of bFGF. See also Figure S7.

SUPPLEMENTAL INFORMATION

Supplemental Information includes seven figures and two videos can be found with this article online at https://doi.org/10.1016/j.celrep.2018.05.083.

ACKNOWLEDGMENTS

The authors thank John Silber and Till Milde for generously providing cell lines and Scott McComb and the Paediatric Leukaemia Group for providing the lenti-CRISPR constructs. Imaging was performed with equipment maintained by the Centre for Microscopy and Image Analysis, University of Zürich. A.S.G.S. is supported by the Garron Family Cancer Research Center at the Hospital for Sick Children and the Worldwide Cancer Research. M.D.T. is supported by the NIH (R01CA148699 and R01CA159859), The Pediatric Brain Tumour Foundation, The Terry Fox Research Institute, The Canadian Institutes of Health Research, The Cure Search Foundation, b.r.a.i.n.child, Meagan's Walk, Genome Canada, Genome BC, Worldwide Cancer Research, V-Foundation for Cancer Research (T2017-020), and the Ontario Institute for Cancer Research through funding provided by the Government of Ontario. M.D.T. is also supported by a Canadian Cancer Society Research Institute Impact grant and by a Stand Up To Cancer (SU2C) St. Baldrick's Pediatric Dream Team Translational Research Grant (SU2C-AACR-DT1113) and SU2C Canada Cancer Stem Cell Dream Team Research Funding (SU2C-AACR-DT-19-15) provided by the Government of Canada through Genome Canada and the Canadian Institutes of Health Research, with supplementary support from the Ontario Institute for Cancer Research through funding provided by the Government of Ontario. Stand Up To Cancer is a program of the Entertainment Industry Foundation administered by the American Association for Cancer Research. M.D.T. is also supported by the Garron Family Chair in Childhood Cancer Research at the Hospital for Sick Children and the University of Toronto. Main funding for this study was provided by the Swiss National Science Foundation (SNF_31004A-144090/1, 165860/1), by the Werner and Hedy Berger-Janser and the Sassella Foundations, by the Swiss Cancer League (CHKL-2834-02-2016), and by Childhood Cancer Switzerland.

AUTHOR CONTRIBUTIONS

K.S.K. planned and conducted experiments and contributed to designing the study, preparing the figures, and writing the manuscript. A.N. established organotypic cerebellar slice culture. A.S.G.S. and C.M.K.-F. performed *in vivo* experiments. D.T. established LA-EGFP-expressing cell lines and supported establishment of sgFRS2 lines. L.B. sorted the sgFRS2 lines. D.K. provided experimental support for brain tissue clearing and imaging. E.J.R. analyzed IHC data. M.D.T. critically reviewed the manuscript. M.A.G. helped to draft the study and critically reviewed the manuscript. M.B. planned and conducted experiments, designed the study, and wrote the manuscript.

DECLARATION OF INTERESTS

The authors declare no competing interests.

Received: October 23, 2017
Revised: March 13, 2018
Accepted: May 24, 2018
Published: June 26, 2018

REFERENCES

Adachi, S., Yasuda, I., Nakashima, M., Yamauchi, T., Yoshioka, T., Okano, Y., Moriwaki, H., and Kozawa, O. (2011). Rho-kinase inhibitor upregulates migration by altering focal adhesion formation via the Akt pathway in colon cancer cells. Eur. J. Pharmacol. *650*, 145–150.

Aref, D., Moffatt, C.J., Agnihotri, S., Ramaswamy, V., Dubuc, A.M., Northcott, P.A., Taylor, M.D., Perry, A., Olson, J.M., Eberhart, C.G., and Croul, S.E. (2013). Canonical TGF-β pathway activity is a predictor of SHH-driven medulloblastoma survival and delineates putative precursors in cerebellar development. Brain Pathol. *23*, 178–191.

Ashcroft, G.S., Yang, X., Glick, A.B., Weinstein, M., Letterio, J.L., Mizel, D.E., Anzano, M., Greenwell-Wild, T., Wahl, S.M., Deng, C., and Roberts, A.B. (1999). Mice lacking Smad3 show accelerated wound healing and an impaired local inflammatory response. Nat. Cell Biol. *1*, 260–266.

Bissell, M.J., and Radisky, D. (2001). Putting tumours in context. Nat. Rev. Cancer *1*, 46–54.

Bouffet, E., Bernard, J.L., Frappaz, D., Gentet, J.C., Roche, H., Tron, P., Carrie, C., Raybaud, C., Joannard, A., Lapras, C., et al. (1992). M4 protocol for cerebellar medulloblastoma: supratentorial radiotherapy may not be avoided. Int. J. Radiat. Oncol. Biol. Phys. *24*, 79–85.

Cavalli, F.M.G., Remke, M., Rampasek, L., Peacock, J., Shih, D.J.H., Luu, B., Garzia, L., Torchia, J., Nor, C., Morrissy, A.S., et al. (2017). Intertumoral heterogeneity within medulloblastoma subgroups. Cancer Cell *31*, 737–754.e6.

Chung, K., Wallace, J., Kim, S.Y., Kalyanasundaram, S., Andalman, A.S., Davidson, T.J., Mirzabekov, J.J., Zalocusky, K.A., Mattis, J., Denisin, A.K., et al. (2013). Structural and molecular interrogation of intact biological systems. Nature *497*, 332–337.

Derynck, R., and Zhang, Y.E. (2003). Smad-dependent and Smad-independent pathways in TGF-beta family signalling. Nature *425*, 577–584.

Emmenegger, B.A., Hwang, E.I., Moore, C., Markant, S.L., Brun, S.N., Dutton, J.W., Read, T.A., Fogarty, M.P., Singh, A.R., Durden, D.L., et al. (2013). Distinct roles for fibroblast growth factor signaling in cerebellar development and medulloblastoma. Oncogene *32*, 4181–4188.

Fiaschetti, G., Shalaby, T., Baumgartner, M., and Grotzer, M.A. (2014). Notch ligands Jag1 and Jag2 control medulloblastoma cell survival and represent potential prognostic markers and therapeutic targets. Neuro-oncol. *16* (*Suppl 1*), i74.

Fogarty, M.P., Emmenegger, B.A., Grasfeder, L.L., Oliver, T.G., and Wechsler-Reya, R.J. (2007). Fibroblast growth factor blocks Sonic hedgehog signaling in neuronal precursors and tumor cells. Proc. Natl. Acad. Sci. USA *104*, 2973–2978.

Friedl, P., and Wolf, K. (2010). Plasticity of cell migration: a multiscale tuning model. J. Cell Biol. *188*, 11–19.

Frühwald, M.C., and Plass, C. (2002). Metastatic medulloblastoma—therapeutic success through molecular target identification? Pharmacogenomics J. *2*, 7–10.

Gotoh, N. (2008). Regulation of growth factor signaling by FRS2 family docking/scaffold adaptor proteins. Cancer Sci. *99*, 1319–1325.

Guagnano, V., Furet, P., Spanka, C., Bordas, V., Le Douget, M., Stamm, C., Brueggen, J., Jensen, M.R., Schnell, C., Schmid, H., et al. (2011). Discovery of 3-(2,6-dichloro-3,5-dimethoxy-phenyl)-1-6-[4-(4-ethyl-piperazin-1-yl)-phenylamino]-pyrimidin-4-yl-1-methyl-urea (NVP-BGJ398), a potent and selective inhibitor of the fibroblast growth factor receptor family of receptor tyrosine kinase. J. Med. Chem. *54*, 7066–7083.

Heldin, C.H., Landström, M., and Moustakas, A. (2009). Mechanism of TGF-beta signaling to growth arrest, apoptosis, and epithelial-mesenchymal transition. Curr. Opin. Cell Biol. *21*, 166–176.

Hetrick, B., Han, M.S., Helgeson, L.A., and Nolen, B.J. (2013). Small molecules CK-666 and CK-869 inhibit actin-related protein 2/3 complex by blocking an activating conformational change. Chem. Biol. *20*, 701–712.

Jacquemet, G., Hamidi, H., and Ivaska, J. (2015). Filopodia in cell adhesion, 3D migration and cancer cell invasion. Curr. Opin. Cell Biol. *36*, 23–31.

Jacquemet, G., Paatero, I., Carisey, A.F., Padzik, A., Orange, J.S., Hamidi, H., and Ivaska, J. (2017). FiloQuant reveals increased filopodia density during breast cancer progression. J. Cell Biol. *216*, 3387–3403.

Jalali, S., Chung, C., Foltz, W., Burrell, K., Singh, S., Hill, R., and Zadeh, G. (2014). MRI biomarkers identify the differential response of glioblastoma multiforme to anti-angiogenic therapy. Neuro-oncol. *16*, 868–879.

Keely, P.J., Conklin, M.W., Gehler, S., Ponik, S.M., and Provenzano, P.P. (2007). Investigating integrin regulation and signaling events in three-dimensional systems. Methods Enzymol. *426*, 27–45.

Keles, G.E., Berger, M.S., Srinivasan, J., Kolstoe, D.D., Bobola, M.S., and Silber, J.R. (1995). Establishment and characterization of four human medulloblastoma-derived cell lines. Oncol. Res. *7*, 493–503.

Kerber, M.L., and Cheney, R.E. (2011). Myosin-X: a MyTH-FERM myosin at the tips of filopodia. J. Cell Sci. *124*, 3733–3741.

Kiltie, A.E., Lashford, L.S., and Gattamaneni, H.R. (1997). Survival and late effects in medulloblastoma patients treated with craniospinal irradiation under three years old. Med. Pediatr. Oncol. *28*, 348–354.

Korobova, F., and Svitkina, T. (2008). Arp2/3 complex is important for filopodia formation, growth cone motility, and neuritogenesis in neuronal cells. Mol. Biol. Cell *19*, 1561–1574.

Lai, M., Guo, Y., Ma, J., Yu, H., Zhao, D., Fan, W., Ju, X., Sheikh, M.A., Malik, Y.S., Xiong, W., et al. (2015). Myosin X regulates neuronal radial migration through interacting with N-cadherin. Front. Cell. Neurosci. *9*, 326.

Liang, Y., Diehn, M., Bollen, A.W., Israel, M.A., and Gupta, N. (2008). Type I collagen is overexpressed in medulloblastoma as a component of tumor microenvironment. J. Neurooncol. *86*, 133–141.

Liu, Y., Yuelling, L.W., Wang, Y., Du, F., Gordon, R.E., O'Brien, J.A., Ng, J.M.Y., Robins, S., Lee, E.H., Liu, H., et al. (2017). Astrocytes promote medulloblastoma progression through hedgehog secretion. Cancer Res. *77*, 6692–6703.

Ma, M., and Baumgartner, M. (2014). Intracellular *Theileria annulata* promote invasive cell motility through kinase regulation of the host actin cytoskeleton. PLoS Pathog. *10*, e1004003.

Maddox, A.S., and Burridge, K. (2003). RhoA is required for cortical retraction and rigidity during mitotic cell rounding. J. Cell Biol. *160*, 255–265.

Margol, A.S., Robison, N.J., Gnanachandran, J., Hung, L.T., Kennedy, R.J., Vali, M., Dhall, G., Finlay, J.L., Erdreich-Epstein, A., Krieger, M.D., et al. (2015). Tumor-associated macrophages in SHH subgroup of medulloblastomas. Clin. Cancer Res. *21*, 1457–1465.

Massagué, J. (2012). TGFβ signalling in context. Nat. Rev. Mol. Cell Biol. *13*, 616–630.

Matsuo, I., and Kimura-Yoshida, C. (2013). Extracellular modulation of fibroblast growth factor signaling through heparan sulfate proteoglycans in mammalian development. Curr. Opin. Genet. Dev. *23*, 399–407.

McComb, S., Aguadé-Gorgorió, J., Harder, L., Marovca, B., Cario, G., Eckert, C., Schrappe, M., Stanulla, M., von Stackelberg, A., Bourquin, J.P., and Bornhauser, B.C. (2016). Activation of concurrent apoptosis and necroptosis by SMAC mimetics for the treatment of refractory and relapsed ALL. Sci. Transl. Med. *8*, 339ra70.

Milde, T., Lodrini, M., Savelyeva, L., Korshunov, A., Kool, M., Brueckner, L.M., Antunes, A.S., Oehme, I., Pekrun, A., Pfister, S.M., et al. (2012). HD-MB03 is a novel group 3 medulloblastoma model demonstrating sensitivity to histone deacetylase inhibitor treatment. J. Neurooncol. *110*, 335–348.

Neve, A., Santhana Kumar, K., Tripolitsioti, D., Grotzer, M.A., and Baumgartner, M. (2017). Investigation of brain tissue infiltration by medulloblastoma cells in an ex vivo model. Sci. Rep. *7*, 5297.

Nobes, C.D., and Hall, A. (1999). Rho GTPases control polarity, protrusion, and adhesion during cell movement. J. Cell Biol. *144*, 1235–1244.

Pei, Y., Liu, K.W., Wang, J., Garancher, A., Tao, R., Esparza, L.A., Maier, D.L., Udaka, Y.T., Murad, N., Morrissy, S., et al. (2016). HDAC and PI3K antagonists cooperate to inhibit growth of MYC-driven medulloblastoma. Cancer Cell *29*, 311–323.

Plackett, R.L., and Burman, J.P. (1946). The design of optimum multifactorial experiments. Biometrika *33*, 305–325.

Quail, D.F., and Joyce, J.A. (2017). The microenvironmental landscape of brain tumors. Cancer Cell *31*, 326–341.

Sahai, E., and Marshall, C.J. (2003). Differing modes of tumour cell invasion have distinct requirements for Rho/ROCK signalling and extracellular proteolysis. Nat. Cell Biol. *5*, 711–719.

Salsman, V.S., Chow, K.K., Shaffer, D.R., Kadikoy, H., Li, X.N., Gerken, C., Perlaky, L., Metelitsa, L.S., Gao, X., Bhattacharjee, M., et al. (2011). Crosstalk between medulloblastoma cells and endothelium triggers a strong chemotactic signal recruiting T lymphocytes to the tumor microenvironment. PLoS One *6*, e20267.

Santhana Kumar, K., Pillong, M., Kunze, J., Burghardt, I., Weller, M., Grotzer, M.A., Schneider, G., and Baumgartner, M. (2015). Computer-assisted quantification of motile and invasive capabilities of cancer cells. Sci. Rep. *5*, 15338.

Santhana Kumar, K., Tripolitsioti, D., Ma, M., Grählert, J., Egli, K.B., Fiaschetti, G., Shalaby, T., Grotzer, M.A., and Baumgartner, M. (2015). The Ser/Thr kinase MAP4K4 drives c-Met-induced motility and invasiveness in a cell-based model of SHH medulloblastoma. Springerplus *4*, 19.

Schwalbe, E.C., Lindsey, J.C., Nakjang, S., Crosier, S., Smith, A.J., Hicks, D., Rafiee, G., Hill, R.M., Iliasova, A., Stone, T., et al. (2017). Novel molecular subgroups for clinical classification and outcome prediction in childhood medulloblastoma: a cohort study. Lancet Oncol. *18*, 958–971.

Shirakihara, T., Horiguchi, K., Miyazawa, K., Ehata, S., Shibata, T., Morita, I., Miyazono, K., and Saitoh, M. (2011). TGF-β regulates isoform switching of FGF receptors and epithelial-mesenchymal transition. EMBO J. *30*, 783–795.

Snoussi, K., Mahfoudh, W., Bouaouina, N., Fekih, M., Khairi, H., Helal, A.N., and Chouchane, L. (2010). Combined effects of IL-8 and CXCR2 gene polymorphisms on breast cancer susceptibility and aggressiveness. BMC Cancer *10*, 283.

Suraneni, P., Rubinstein, B., Unruh, J.R., Durnin, M., Hanein, D., and Li, R. (2012). The Arp2/3 complex is required for lamellipodia extension and directional fibroblast cell migration. J. Cell Biol. *197*, 239–251.

Taylor, M.D., Northcott, P.A., Korshunov, A., Remke, M., Cho, Y.J., Clifford, S.C., Eberhart, C.G., Parsons, D.W., Rutkowski, S., Gajjar, A., et al. (2012). Molecular subgroups of medulloblastoma: the current consensus. Acta Neuropathol. *123*, 465–472.

Thoma, C.R., Zimmermann, M., Agarkova, I., Kelm, J.M., and Krek, W. (2014). 3D cell culture systems modeling tumor growth determinants in cancer target discovery. Adv. Drug Deliv. Rev. *69-70*, 29–41.

Torka, R., Thuma, F., Herzog, V., and Kirfel, G. (2006). ROCK signaling mediates the adoption of different modes of migration and invasion in human mammary epithelial tumor cells. Exp. Cell Res. *312*, 3857–3871.

Turner, N., and Grose, R. (2010). Fibroblast growth factor signalling: from development to cancer. Nat. Rev. Cancer *10*, 116–129.

Wei, L., Surma, M., Shi, S., Lambert-Cheatham, N., and Shi, J. (2016). Novel insights into the roles of Rho kinase in cancer. Arch. Immunol. Ther. Exp. (Warsz.) *64*, 259–278.

Wells, A., Kassis, J., Solava, J., Turner, T., and Lauffenburger, D.A. (2002). Growth factor-induced cell motility in tumor invasion. Acta Oncol. *41*, 124–130.

Wu, X., Northcott, P.A., Dubuc, A., Dupuy, A.J., Shih, D.J., Witt, H., Croul, S., Bouffet, E., Fults, D.W., Eberhart, C.G., et al. (2012). Clonal selection drives genetic divergence of metastatic medulloblastoma. Nature *482*, 529–533.

Yang, S., and Kim, H.M. (2014). ROCK inhibition activates MCF-7 cells. PLoS One *9*, e88489.

Yang, F., Liu, Y., Tu, J., Wan, J., Zhang, J., Wu, B., Chen, S., Zhou, J., Mu, Y., and Wang, L. (2014). Activated astrocytes enhance the dopaminergic differentiation of stem cells and promote brain repair through bFGF. Nat. Commun. *5*, 5627.

Zhang, Y.E. (2009). Non-Smad pathways in TGF-beta signaling. Cell Res. *19*, 128–139.

Zhou, W., Feng, X., Wu, Y., Benge, J., Zhang, Z., and Chen, Z. (2009). FGF-receptor substrate 2 functions as a molecular sensor integrating external regulatory signals into the FGF pathway. Cell Res. *19*, 1165–1177.

STAR★METHODS

KEY RESOURCES TABLE

REAGENT or RESOURCE	SOURCE	IDENTIFIER
Antibodies		
Anti-bFGF	Santa Cruz Biotechnology	Sc-79
Anti-FGFR1	Abcam	Ab10646
Anti-GFAP	Abcam	Ab53554
Anti-calbindin	Abcam	Ab11426
Anti-phospho ERK1/2	Cell signaling technologies	9101
Anti-phospho ERK1/2 (Thr202/Tyr204)	Cell signaling technologies	4370
Anti-ERK1/2	Cell signaling technologies	9102
Anti-phospho FRS2 (Y436)	Cell signaling technologies	3861S
Anti-ROCK1	Cell signaling technologies	4035
Anti-phospho-PKC (pan βII Ser660)	Cell signaling technologies	9371
Anti-MYPT1	Cell signaling technologies	2634
Anti-mouse horseradish peroxidase (HRP) linked	Cell signaling technologies	7076
Anti-rabbit HRP linked	Cell signaling technologies	7074
Anti-TGF-β1	SantaCruz	sc146
Anti-TGF-β-R1	Abcam	ab31013
Anti-TGF-β-R2	Abcam	ab61213
Anti-FRS2/SNT-1	Merck millipore	05-502
Anti-ROCK2	Merck millipore	ABS436
Anti-phospho MYPT1 (Thr696)	Merck millipore	ABS45
Anti-phospho tyrosine (4G10 platinum)	Merck millipore	05-1050
Anti-myosin-X	Sigma Aldrich	HPA024223
Anti-tubulin	Sigma Aldrich	T9026
Anti-human nuclei	Merck millipore	MAB4383
Anti-rabbit-Cy3-coupled	Jackson immuno research	711-165-152
Anti-mouse-Cy5-coupled	Jackson immuno research	415-175-166
Anti-VASP	Sigma Aldrich	HPA005724
Bacterial and Virus Strains		
LentiCRISPR	(McComb et al., 2016)	N/A
pVSV	Oliver Pertz	N/A
pMDL	Oliver Pertz	N/A
pRev	Oliver Pertz	N/A
pLA-EGFP	Oliver Pertz	N/A
Biological Samples		
A Tissue Microarray (TMA) with anonymized, validated MB and cerebellum samples (tumor: male: 32, female: 17, unknown: 23, cerebellum: male: 6, female: 1) was used.	University Hospital Zürich	N/A
Paraffin embedded anonymized, validated human medulloblastoma tissue sections.	University Hospital Zürich	N/A
Paraffin embedded human medulloblastoma Patient-derived Xenograft tissue sections	SickKids Hospital, Toronto, Canada	N/A
Chemicals, Peptides, and Recombinant Proteins		
basic Fibroblast Growth Factor	PeproTech	100-18B
Transforming Growth Factor-β	PeproTech	100-21

(*Continued on next page*)

Continued

REAGENT or RESOURCE	SOURCE	IDENTIFIER
Hepatocyte growth factor	PeproTech	100-39
Epidermal growth factor	PeproTech	100-47
Netrin	R&D Systems	6419-N1-025
Insulin like Growth Factor 1	PeproTech	100-11
Platelet Derived Growth Factor-B	PeproTech	P100-14B
Tumor Necrosis Factor-α	PeproTech	300-01A
Interleukin-6	PeproTech	200-06
Nerve Growth Factor-β	PeproTech	450-01
Placental Growth Factor-1	PeproTech	100-06
ML141	Selleckchem	S7686
SCH772984	Selleckchem	S7101
BGJ398	Selleckchem	S2183
SP600125	Selleckchem	S1460
U0126	Selleckchem	S1102
LY294002	Selleckchem	S1105
IPA-3	Selleckchem	S7093
Go6983	Selleckchem	S2911
NSC23766	Selleckchem	S8031
CCG-1423	Selleckchem	S7719
Y-27632	Selleckchem	S1049
LY2157299	Selleckchem	S2230
H-1152	Alexis Biochemicals	ALX-270-423
CK666	Sigma Aldrich	SML0006
Mitomycin C	Sigma Aldrich	M4287
Blebbistatin	Sigma Aldrich	B0560
hexadimethrine bromide	Sigma Aldrich	H9268
Hoechst	Sigma Aldrich	B2883
Pure coll bovine collagen 1	Cell systems	5005-B
Cell proliferation WST-1 reagent (Roche)	Sigma Aldrich	11644807001
Glycergel	Dako	C0563
Critical Commercial Assays		
G-LISA Rac1 activation kit	Cytoskeleton	BK128
G-LISA Cdc42 activation kit	Cytoskeleton	BK127
G-LISA RhoA activation kit	Cytoskeleton	BK124
RNeasy Mini RNA isolation kit	QIAGEN	74106
High capacity cDNA reverse transcription kit	Applied biosystems	4368814
Experimental Models: Cell Lines		
DAOY, Desmoplastic MB, age of patient: 4 years, gender: male, authenticated using genotyping	ATCC	ATCC: HTB-186
UW228, MB, age of patient: 9 years, gender: female, authenticated by genotyping compared to original tumor line UW228-2.	John Silber, Seattle, USA	(Keles et al., 1995)
HD-MBO3, group 3 MB, age of patient: 3, gender: male	Till Milde, Heidelberg, Germany	(Milde et al., 2012)
Med311 PDX TC adapted, MB, age of patient: 2 years, gender: male	Brain tumor resource laboratory of the Fred Hutchinson Cancer Centre	http://www.btrl.org/product/med-311fhtc/
Med 114 PDX, Med 411 PDX, Med 411 GFP PDX, Anaplastic, Large cell MB, age of patient: 3 years, gender: male	SickKids Hospital, Toronto, Canada	http://www.btrl.org/product/med-411fh/

(*Continued on next page*)

Continued

REAGENT or RESOURCE	SOURCE	IDENTIFIER
Med 1712 PDX, Desmoplastic/Nodular Grade IV MB, age of patient: 4 years, gender: male	Brain tumor resource laboratory of the Fred Hutchinson Cancer Centre	http://www.btrl.org/product/med-1712fh/
D341 PDX, group 3 MB, age of patient: 3.5 years, gender: male	SickKids Hospital, Toronto, Canada	N/A
Experimental Models: Organisms/Strains		
Mice for *ex vivo* experiments – C57BL/6JRj, pregnant female, male and female pubs were used for brain dissection. Sex of pubs was not determined and slices were randomized.	Janiver labs	N/A
Mice for *in vivo* experiments – NOD SCID gamma (NGS), all male, average weight at experiment start was 28.23 g -/+ 2.76. Age of mice used at start of experiment: seven weeks.	Breeders purchased from Jackson laboratories, bred by University Health Network	https://www.jax.org/strain/005557 https://navigator.innovation.ca/en/navigator/AnimalResourcesCentre
Oligonucleotides		
sgFRS2, Exon 1, AACTTGTTCCGATGGTTATCTGG	This paper	N/A
sgFRS2, Exon 2, TACCTCTGCCTGCGACGCTATGG	This paper	N/A
sgFRS2, Exon 3, TAGGTGTTCGAGGTGTTCTAGGG	This paper	N/A
sgFRS2, Exon 4, AGGATGTCTGCTTGACGGATGGG	This paper	N/A
Software and Algorithms		
Automated cell dissemination counter (aCDc) platform. Automated spheroid dissemination counter software (asDICs) used for quantification.	Kumar et al., 2015	http://www.infozentrum.ethz.ch/uploads/user_upload/Software/ImageAnalysisSoftware.zip
R2 microarray	Santhana Kumar et al., 2015 and this paper	http://r2.amc.nl

CONTACT FOR REAGENT AND RESOURCE SHARING

Further information and request for resources and reagents should be directed to and will be fulfilled by the Lead Contact, Martin Baumgartner, Martin.Baumgartner@kispi.uzh.ch.

EXPERIMENTAL MODEL AND SUBJECT DETAILS

Human Subjects

Informed consent was obtained from subjects and all research involving subject's material was conducted under appropriate review/privacy board protocols of the Kantonale Ethikkommission Zürich (Ethics Commission of the Canton of Zürich, Switzerland). The use of patient tumor material for diagnostic and prognostic analysis was approved by the Kantonale Ethikkommission Zürich.

Mouse Maintenance

Mouse protocols for organotypic brain slice culture were approved by the Veterinary Office of the Canton Zürich. Wild-type C57BL/6JRj pregnant females were purchased from Janvier Labs and were kept in the animal facilities of the University of Zürich Laboratory Animal Center. *In vivo* experiments in NSG mice were approved by the institutional animal care committee at University Health Network, Toronto.

TISSUE CULTURE CELLS

Human MB Cell Lines

DAOY human MB cells were purchased from the American Type Culture Collection (ATCC, Rockville, MD, USA). UW228 (Keles et al., 1995) was generously provided by John Silber (Seattle, USA). DAOY and UW228 cells were cultured as described in (Fiaschetti et al., 2014). DAOY LA-EGFP and UW228 LA-EGFP cells were produced by lentiviral transduction of DAOY and UW228 cells with pLenti-LA-EGFP. Cell line authentication and cross contamination testing was performed by Multiplexion by single nucleotide polymorphism (SNP) profiling.

Patient-Derived Xenograft (PDX) Cell Culture

Human MB SHH PDX line Med-1712FH, human MB Group 3 line Med-411FH and human atypical MB line Med311PDX were obtained from the brain tumor resource laboratory of the Fred Hutchinson Cancer Centre. Group 3 line HD-MBO3 was a generous gift of Till Milde (Heidelberg, Germany) and cultivated in RPMI 1640 medium supplemented with 10% heat-inactivated fetal calf serum and 1% nonessential amino acids. Med-1712FH and Med-411FH cells were cultured in neurobasal medium (Invitrogen/Life Technologies, Paisley, UK, 12349-015) supplemented with 2% B-27® (GIBCO/Life Technologies, 10889-038), 1% L-Glutamine (Invitrogen/Life Technologies, 25030024), 10 μg/ml bFGF (100-18B, PeproTech, London, UK) and 10 μg/ml EGF (100-47, PeproTech, London, UK). Med311PDX cells were cultured in NeuroCult NS-A Basal Medium (Human) with NeuroCult NS-A proliferation supplements (Human) (05751, Stem Cell Technologies), 10 μg/ml bFGF (100-18B, PeproTech, London, UK), 10 μg/ml EGF (100-47, PeproTech, London, UK) and 1% Penicillin/Streptomycin (15140122, GIBCO by Life Technologies) on laminin (L2020-1MG, Sigma-Aldrich, dilute 1mg/ml laminin (1:100) in PBS) coated tissue culture treated dishes.

METHODS DETAILS

Inhibitors

Inhibitors were used throughout the study at concentrations indicated in Figure S2A, unless otherwise specified. ML141 (S7686), SCH772984 (S7101), BGJ398 (S2183), SP600125 (S1460), U0126 (S1102), LY294002 (S1105), IPA-3 (S7093), Go6983 (S2911), NSC23766 (S8031), CCG-1423 (S7719), Y-27632 (S1049), LY2157299 (S2230) were purchased from Selleckchem, Houston, TX, USA. H-1152 (ALX-270-423, Alexis Biochemicals), CK666 (SML0006, Sigma Aldrich), blebbistatin (B0560, Sigma Aldrich).

Spheroid Invasion Assay (SIA) and Automated Cell Dissemination Counter (aCDc)

1000 cells/100 μL per well were seeded in 96 well Corning® Spheroid microplate (CLS4520, Sigma-Aldrich) (DAOY cells) or in cell-repellent 96 well microplate (650790, Greiner Bio-one) (UW228, Med311PDX, Med411FH and Med1712FH). For SIA with proliferation inhibition, cells pre-treated with 10 μM of mitomycin for 3 h were used. The cells were incubated at 37°C overnight to form spheroids. 70 μl of the medium were removed from each well, and remaining medium with spheroid overlaid with 2.5% bovine collagen 1. Following the polymerization of collagen, fresh medium was added to the cells and treated with growth factors / cytokines and/or with inhibitors. The cells were allowed to invade the collagen matrix for 24 h, after which they were fixed with 4% PFA and stained with Hoechst. Images were acquired on an Axio Observer 2 mot plus fluorescence microscope (Zeiss, Munic, Germany) using a 5x objective. Cell invasion is determined as the average of the distance invaded by the cells from the center of the spheroid as determined using automated cell dissemination counter (aCDc) with our cell dissemination counter software aSDIcs (Kumar et al., 2015).

Expression Analysis Using R2 Database

Expression of FRS2 in normal brain, normal cerebellum and MB samples were analyzed using the open access platform R2 for visualization and analysis of the microarray data (http://r2.amc.nl) as described in (Santhana Kumar et al., 2015). The following datasets were used: Normal brain regions – 172 – MAS5.0 – u133p2 (172 samples, post-mortem brain tissue collected from ADRC brain banks), Normal cerebellum – Roth – 9 – MAS5.0 – u133p2 (9 samples), MB (SHH) Pfister – 76 – u133p2 (73 pediatric MB samples), MB ependymoma – denBoer – 51 – u133p2 (51 samples), MB PLoS One – Kool – 62 – MAS5.0 – u133p2 (62 human MB tumor samples), MB public – Delattre – u133p2 (57 samples), Tumor MB – Gilbertson – 76 – u133p2 (76 samples) and Tumor Glioma pediatric – Paugh – 53 – u133p2 (53 samples).

FRS2 Depletion by LentiCRISPR

BFP tagged LentiCRISPR plasmids were generously provided by Dr. Scott McComb (Ottawa, Canada). Cloning of sgRNA into LentiCRISPR plasmids was performed with a single-tube restriction and ligation method as described in (McComb et al., 2016). Production of lentiviral vectors was performed according to the standard protocol. In brief, 293T cells were transfected with using HEPES-buffered saline solution (HeBS) and 0.5 M calcium phosphate with LentiCRISPR, pVSV, pMDL, and pRev (Kindly provided by Dr. Oliver Pertz, Bern, Switzerland) in a ratio of 4.5:1.5:3:1. The media was changed after 12 h and the virus was collected at 72 h after transfection of plasmids. Viral transductions were performed using hexadimethrine bromide (H9268, Sigma-Aldrich). sgRNA sequences were screened for FRS2 activity in DAOY cells by IB. The most effective sequence was chosen for further experiments. The specific sg target sequences used are listed below:

Gene	Exon	Sg target sequence
FRS2	Exon1	AACTTGTTCCGATGGTTATCTGG
FRS2	Exon2	TACCTCTGCCTGCGACGCTATGG
FRS2	Exon3	TAGGTGTTCGAGGTGTTCTAGGG
FRS2	Exon4	AGGATGTCTGCTTGACGGATGGG

Cell Proliferation WST-1 Assay

The metabolic activity and the proliferation of the cells were determined using the WST-1 assay kit – Roche (11644807001, Sigma Aldrich) according to the manufacturer's instructions. In brief, 2500 cells/100 μl/per well (for up to 72 h incubation) and 750 cells/100 μl/per well (for up to 120 h) were seeded in Greiner Bio-One μ-clear 96 well plates (655090, Greiner Bio-One) and incubated overnight at 37°C. For WST-1 assay with proliferation inhibition, cells pre-treated with 10uM of mitomycin for 3 h were used. The old media was then replaced with fresh serum-free media and the cells were treated with growth factors, inhibitors and/or combinations till the desired time point. Following appropriate incubation for each time point, 10 μL of the WST-1 reagent was added to each well (final concentration of WST-1 reagent per well is 1:10) and incubated at 37°C for 30 min. The absorbance was then measured at 440 nm.

G-LISA

The activity of Rac1, Cdc42 and RhoA in collagen-embedded cells were determined using the G-LISA Rac1 (BK128), Cdc42 (BK127) and RhoA (BK124) G-LISA activation kits (Cytoskeleton), respectively. 2 million cells/ml per well were seeded in 6 well cell repellent plates (657970, Greiner Bio-one) and incubated overnight at 37°C. Cell clusters were embedded in collagen I (final concentration 3 mg/ml) (5005-B, Cellsystems). Fresh medium was added to the cells after polymerization of collagen I. DAOY sgControl and DAOY sgFRS2 collagen-embedded cell clusters were treated with bFGF (100 ng/ml or 10 μg/ml), TGF-β (20 ng/ml), and in various combinations thereof for 24 h. UW228 cell clusters were treated as DAOY cells described above without or with BGJ398 for 24 h. Clusters were lysed and the total protein was isolated as described in (Keely et al., 2007). The levels of GTP-loaded Rac1, Cdc42 and RhoA in the lysates were determined by G-LISA activation kit.

G-LISA—3D, IB

Total protein was isolated from the collagen embedded cell clusters as explained above (G-LISA). Lysates were boiled with the loading buffer (Roti® - Load1, K929.1, Carl Roth, Germany) and analyzed by IB.

Growth Factor Treatments

Growth factors were used throughout the study in the concentrations indicated as follows. basic Fibroblast Growth Factor (bFGF, 100-18B): 100 ng/ml (low, *in vitro*), 10 μg/ml (high, *in vitro*), 12.5 ng/ml (low, OCSC), 100 ng/ml (high, OCSC), Transforming Growth Factor-β (TGF-β, 100-21): 20 ng/ml, Hepatocyte growth factor (HGF, 100-39): 20 ng/ml, epidermal growth factor (EGF, 100-47): 30 ng/ml from PeproTech (London, UK). The following growth factors/cytokines were used for PB design: Netrin (R&D Systems, 6419-N1-025), HGF, EGF, Insulin like Growth Factor 1 (IGF, 100-11), Platelet Derived Growth Factor-B (PDGF-B, P100-14B), Tumor Necrosis Factor-α (TNF- α, 300-01A) bFGF, Interleukin-6 (IL-6, 200-06), Nerve Growth Factor-β (NGF, 450-01), TGF-β and Placental Growth Factor-1 (PlGF-1, 100-06) from PeproTech (London, UK). The concentrations used for 'high' and 'low' levels of the respective growth factors are listed below:

Growth Factor/Cytokine	High Level for PB design	Low Level for PB design
HGF	20ng/ml	0.039ng/ml
Netrin	200ng/ml	0.78ng/ml
EGF	30ng/ml	0.05ng/ml
TNF-α	25ng/ml	0.0975ng/ml
IGF	20ng/ml	0.039ng/ml
PDGF-B	20ng/ml	0.039ng/ml
TGF-β	20ng/ml	0.039ng/ml
IL-6	20ng/ml	0.039ng/ml
NGF	50ng/ml	0.195ng/ml
bFGF	100ng/ml	0.39ng/ml
PlGF-1	10ng/ml	0.078ng/ml

In Vivo Experiments and Imaging

Med-411-FH cells were transduced with a GFP lentiviral expression construct and sorted by FACS. 5×10^5 GFP-positive Med-411-FH cells were stereotaxically injected into the cerebella of 7-week-old NSG mice (n = 18). To detect tumor engraftment, mice were imaged by MRI using a 7 Tesla Biospec 70/30 (Bruker Corporation) as previously described (Jalali et al., 2014) at 21 and 28 days post injection. T2-weighted images were analyzed and at the first signs of tumor engraftment mice were randomized into treatment (n = 5) and control groups (n = 6) and received BGJ398 (in 2:1 PEG300/D5W) 10 mg/kg or vehicle alone daily via oral gavage for 10 doses. Deeply anesthetized mice were then perfused with ice-cold phosphate buffered hydrogel solution containing 4% bis-Acrylamide and

1% w/v paraformaldehyde as published (Yang et al., 2014). Brains were incubated in ice-cold hydrogel solution for 24 h followed by degassing and polymerization at 37°C. Brains were stored and electrophoretically cleared in 8% w/v sodium-dodecyl-sulfate solution (Chung et al., 2013; Yang et al., 2014). Samples were washed in phosphate buffered saline followed by equilibration in refractive index matching solution (RIMS) (Yang et al., 2014). Cleared brains were inserted into 10X10mm high precision optical glass cuvettes (Z802980, Sigma Aldrich) and completely submerged in RIMS.

Confocal image analysis was performed with 488 nm excitation wavelength and Z stacks (35 μm Z-intervals) covering the whole brain area were acquired. The cumulative area of the GFP signal was quantified. The distance of individually invading GFP-positive tumor cells from the local main tumor mass was quantified using ImageJ in μm by drawing a perpendicular line from the tumor mass margin to the cell.

Confocal Immunofluorescence Analysis (IFA)

Single Cells (2D)

8 well ibidi plates were coated with collagen (1:10 in 60% EtOH) and left in the incubator at 37°C overnight. The following day, approximately 500 cells / 200 μL per well is seeded on the collagen coated ibidi plates. 24 h after seeding, the medium was removed and the cells were treated with bFGF for 10 h. The cells were fixed and treated as described in (Ma and Baumgartner, 2014). The fixed cells were incubated with diluted primary antibodies overnight at 4°C. Anti-rabbit-Cy3 – (711-165-152) coupled secondary antibody was diluted 1:300 and incubated for 2 h at RT. Z stacks of the cells were acquired using a 63X immersion objective in SP8 Leica confocal microscope. pERK was quantified on images generated from confocal microscopy image acquisitions with identical settings between samples. Cumulated gray values of the pERK signals were acquired along a 100 pixel length X 100 pixel wide lane perpendicular to the cell margin. The line was cantered on the margin. The cumulated values of multiple measurements per sample were plotted against distance in pixels.

Single Cells on Thick Collagen Layer (Semi 3D)

150 μL of 2.5% bovine collagen I prepared with 7.5% sodium bicarbonate and 10X DMEM medium was added to each well on 8 well ibidi plates and left in the incubator at 37°C for 1 h. Following the polymerization of collagen, 1000 cells/150 μL per well were seeded on the collagen layer. 24 h after seeding, the medium was removed and the cells were treated with bFGF for 18 h. The cells were fixed and treated as described in (Ma and Baumgartner, 2014). Fixed cells were incubated with diluted primary antibodies overnight at 4°C. Anti-rabbit-Cy3 – (711-165-152) coupled secondary antibody was diluted 1:300 and incubated for 2 h at RT. Z stacks of the cells were acquired using a 63X immersion objective with a SP8 Leica confocal microscope.

Spheroids (3D)

DAOY LA-EGFP cells were used to perform SIA in 8 well ibidi plate as described in (Kumar et al., 2015). The embedded spheroids are treated with bFGF, TGF-β, bFGF+TGF and/or Y27632 for 24 h at 37°C. The medium was then removed without disturbing the collagen layer and the collagen I embedded spheroids were fixed with 4% ice cold PFA and permeabilized with 0.5% Triton X-100 for 5 min. The fixed and permeabilized cells were incubated with diluted anti-myosinX antibody overnight at 4°C. Anti-rabbit-Cy3 – (711-165-152) coupled secondary antibody was diluted 1:300 and incubated for 2 h at RT. The spheroids were subsequently stained with Hoechst 1:5000 (B2883, Sigma-Alrich) and mounted with glycergel (Dako, C0563). Z stacks of invaded cells were acquired using 63X immersion objective in SP8 Leica confocal microscope. The total number of cells per region of interest (in each experiment, 6 regions were quantified per sample and condition) and the number of cells displaying filopodia-like structures were counted and the percentage of cells with filopodia-like structures was calculated.

Organotypic Cerebellar Slice Culture (OCSC)

After PFA fixation, the slices were incubated in standard cell culture trypsin EDTA and incubated at 37°C humidified incubator for 23 min. The slices were blocked in PBS containing 3% fetal calf serum, 3% bovine serum albumin and 0.3% triton x 100 for 1 hr at RT. Primary antibodies were diluted in the blocking solution and incubated overnight on a shaker at 4°C. Following 3 washes at RT using 5% BSA in PBS, secondary antibodies were incubated for 3 h at RT. The inserts were flat mounted in glycergel mounting medium (C0563, Dako). The slice-spheroid co-cultures were stained for GFAP and calbindin and three-color image acquisition was performed on a SP8 confocal microscope.

Confocal Live-Cell Imaging—SIA

The embedded spheroids as described in (Kumar et al., 2015) were incubated with bFGF (100 ng/ml; Video S1) or TGF-β (20 ng/ml; Video S2) 10 h prior to the start of image acquisition using SP8 Leica confocal microscope. A multi-immersion 63X objective was used to acquire Z stacks of single invading cells (1 min interval, 15 min acquisition). Average density projections of the stacks were assembled into AVI movies (15 fps).

Immunoblotting (IB)

RIPA buffer lysates were resolved by SDS-PAGE and transferred to a nitrocellulose membrane using a transfer apparatus according to the manufacturer's instructions (Bio-Rad). Membranes were probed with primary antibodies against phospho-FRS2, FRS2, ERK1/2, phospho-ERK1/2, MYPT1, phosphor-MYPT1, phospho-PKC and tubulin. HRP-linked secondary antibodies (1:5000)

were used to detect the primary antibodies. Chemiluminescence detection was performed using ChemiDoc Touch Gel and Western Blot imaging system (BioRad) and FujiFilm LAS 3000 (Bucher biotech) Integrated density of Immuno-reactive bands was quantified using Adobe Photoshop CS3.

Immunohistochemistry (IHC)

IHC of the TMA and normal brain sections was performed by Sophistolab (Muttenz, Switzerland) on a Lecia BondMax instrument using Refine HRP-Kits (Leica DS9800). All buffer solutions were purchased from Lecia Microsystems Newcastle, Ltd and used according to the manufacturer's guidelines. Paraffin-slides were de-waxed, pre-treated and incubated as follows: ER-solution 2 for 10 min at 95°C, ER-solution 2 for 20 min at 100°C and ER-solution 2 for 30 min at 100°C. The TMA slides were captured digitally using Axio Observer 2 mot plus fluorescence microscope (Zeiss, Munich, Germany). The expression of bFGF and FGFR1 was assessed independently at 5x to 20x magnifications. The samples in the TMA slides were classified by H scores by the assessor, who was blind to the clinicopathological data of the patients as high, moderate, low, and negative expression of bFGF and FGFR1. Antibodies used for

Immunoprecipitation

Serum starved cells were incubated with bFGF (*in vitro* low), TGF-β, bFGF (*in vitro* low) + TGF-β and / or SCH772894 for 10 min or bFGF (*in vitro* high), TGF-β, bFGF (*in vitro* high) + TGF-β and / or SCH772894 for 24 h. The cells were lysed with 0.5% NP40 lysis buffer without SDS and the protein concentrations were normalized among the samples. Anti-FRS2 antibody is incubated with 100 μL of Dynabeads® Protein G beads (10003D, Thermofischer Scientific) and 200 μL of PBST for 30 min on an Eppendorf rotator at RT. The antibody-bead complex was isolated using the immunoprecipitation magnet (Merck Millipore). The equalized lysates were incubated with anti-FRS2-bead complex for 1 to 2 h at 4°C. The immune complexes were eluted from the beads by boiling the samples to 95°C with the loading buffer (Roti® - Load1, K929.1, Carl Roth, Germany) and were analyzed by IB as described above. Antibodies and concentrations used for IFA, IB, IHC and IP are listed below:

Primary Antibody	Dilution	Application
bFGF	1:400	Immunohistochemistry
FGFR1	1:100	Immunohistochemistry
TGF-β	1:100	Immunohistochemistry
TβRI	1:50	Immunohistochemistry
TβRII	1:500	Immunohistochemistry
pERK1/2	1:750	Immunoblot
pERK1/2 (Thr202/Tyr204)	1:250	Immunoflurorescence
ERK1/2	1:1000	Immunoblot
pFRS2 (Y436)	1:750	Immunoblot
FRS2	1:1000	Immunoblot
FRS2	4 μg of antibody for 500-1000 μg/ml of protein	Immunoprecipitation
Myosin-X	1:250	Immunofluorescence
ROCK1	1:1000	Immunoblot
ROCK2	1:1000	Immunoblot
pMYPT1 (Thr696)	1:500	Immunoblot
MYPT1	1:750	Immunoblot
RhoA	1:250	G-LISA
Rac1	1:20	G-LISA
Cdc42	1:50	G-LISA
Phospho-tyrosine, pTyr (4G10)	1:1000	Immunoblot
GFAP	1:300	Immunofluorescence
Calbindin	1:1000	Immunofluorescence
pPKC	1:750	Immunoblot
Tubulin	1:1000	Immunoblot
VASP	1:250	Immunofluorescence

Organotypic Cerebellar Slice Culture

Wild-type C57BL/6JRj mice pups were sacrificed at postnatal day (PND) 8-10 by decapitation. Cerebella were dissected and placed in cold Geys balanced salt solution containing kynurenic acid (GBSSK) and then embedded in 2% low melting point agarose gel. Solidified agarose blocks were glued onto the vibratome (VT 1200S, Leica) disc with Roti Coll1 glue (0258.1 Carl Roth), mounted in the vibratome chamber filled with cold GBSSK and 350 μm thick sections were cut. Slices were transferred to Petri dishes filled with cold GBSSK. Millipore inserts (PICM 03050, Merck Millipore) were placed in six well plate(s) filled with 1 mL cold slice culture medium (SCM) onto which the slices were then transferred using a Rotilabo-embryo spoon (TL85.1, Carl Roth). A maximum of three slices were placed per insert and excess of medium was removed. Slices were monitored for any signs of apoptosis and media was changed daily for the first week and once in two days thereafter. Tumor spheroids were formed with DAOY LA-EGFP cells, DAOY sgControl cells and DAOY sgFRS2 cells. The co-culture was treated with bFGF (OCSC low and OCSC high), TGF-β, bFGF (OSCS high) + TGF-β and / or BGJ398. Spheroids were incubated for 7 or 5 days for DAOY sgControl and DAOY sgFRS2 or control and BGJ398-treated, respectively. Following the treatment, the co-cultures were fixed as described in (Neve et al., 2017). The fixed co-cultures were stained and analyzed using immunofluorescence techniques. The distance of dissemination of MB cells from the center of the spheroid in the co-culture were quantified using modified aSDIcs.

PB Design

Plackett Burman (PB) design, an orthogonal screening matrix that yields unbiased estimates of all independent variables in the smallest design possible, was adapted to perform the combinatorial growth factor screen (Plackett and Burman, 1946). Multiple growth factors affect MB cell dissemination simultaneously. PB is based on Two-level (High and Low) Hadamard screening matrices where 'n' variables (number of growth factors to be tested = 11) can be tested in 'n+1' runs. The 11 growth factors that were tested in combinations of high and low levels were as follows: HGF, EGF, Netrin, TNF-α, IGF, PDGF-B, TGF-β, IL-6, bFGF, NFG and PlGF-1. The PB screening matrix for 12 runs is shown in Figure S5A. The high levels of the growth factors / cytokines are represented as "+" and those in low levels are represented as "−". The high and low levels of the 11 growth factors / cytokines screened were determined by 1:2 serial dilution. The minimum concentration of the growth factor required to induce a measureable level (statistically significant) of cell dissemination as compared to the control was set as the low level of the growth factor / cytokine.

RNA Expression Analysis by qRT-PCR

Total RNA was isolated using RNeasy Mini Kit (QIAGEN, Basel, Switzerland) following the manufacturer's instructions. 100 ng of total RNA was used as a template for reverse transcription, which was initiated by random hexamer primers. The cDNA synthesis was carried out using High capacity cDNA Reverse Transcription Kit (Applied Biosystems). qRT-PCR was performed under conditions optimized for the ABI7900HT instrument, using TaqMan® Gene Expression Master Mix (4369016, Applied Biosystems). Primer probes specific for the following genes (4331182, Applied Biosystems) were used: FGFR1 (Hs00915142_m1), FGFR2 (Hs01552926_m1), FGFR3 (Hs00179829_m1), FGFR4 (Hs01106908_m1), FGF2 (Hs00266645_m1), TGF-β1 (Hs00998133_m1), TGFBR1 (Hs00610320_m1), TGFBR2 (Hs00234253_m1) and TGFBR3L (Hs00418521_m1). Cycle threshold (CT) values were normalized to housekeeping gene GAPDH (Hs02758991_g1, Applied Biosystems). ΔΔCT method was used to calculate the relative gene expression of each gene of interest.

RNA Interference

Approximately 75% confluent cells were transfected with siRNA specific for ERK1 (MAPK3 – ID: s11140), ERK2 (MAPK1 – ID: s11137), ROCK1 (ID: s12097), ROCK2 (ID: s18163), FRS2 (ID: s21261) or Silencer select negative control (ID: 4390843, Ambion). Each siRNA was used at a final concentration of 5 nmol along with DharmaFECT 4 transfection regent (T-2004-03, Dharmacon). After 48 h, RNA and proteins were isolated from cells to determine gene expression by qRT-PCR and protein expression by IB. On successful downregulation of the protein of interest, the transfected cells were used for SIA.

QUANTIFICATION AND STATISTICAL ANALYSIS

Mean ± SD are shown when means of three biological replicas (n = 3) are compared. Boxplots with whiskers to min and max are shown when pooled individual measurements from two to three biological replicas are compared. Unpaired Student's t test was used to test significance of differences between two samples acquired in each of three biological replicas. For all other analyses, one-way ANOVA repeated-measures test using Bonferroni's Multiple Comparison using Prism software was performed. p values < 0.05 were considered significant (* $p \leq 0.05$, ** $p \leq 0.01$, *** $p \leq 0.001$), **** $p \leq 0.0001$). Where indicated, asterisks show statistical significances between control and test sample.